

A MECHANISTIC INVESTIGATION OF THE AROA REACTION

UNDERSTANDING THE AROA MECHANISM:
EVIDENCE FOR ENOLPYRUVYL ACTIVATION AND KINETIC ISOTOPE
EFFECT MEASUREMENTS

By

MEGHANN E. CLARK, B. Sc.

A Thesis

Submitted to the School of Graduate Studies

in Partial Fulfillment of the Requirements

for the Degree

Master of Science

McMaster University

© Copyright by Meghann E. Clark, August 2006

MASTER OF SCIENCE (2006)

McMaster University

(Biochemistry and Biomedical Sciences)

Hamilton, Ontario

TITLE: Understanding the AroA Mechanism: Evidence for
*Enol*pyruvyl Activation and Kinetic Isotope Effect
Measurements

AUTHOR: Meghann E. Clark, B. Sc. (McMaster University)

SUPERVISOR: Dr. Paul J. Berti

NUMBER OF PAGES: xi, 78

Abstract

AroA catalyzes a carboxyvinyl transfer reaction, forming *enol*pyruvyl shikimate 3-phosphate (EPSP) from shikimate 3-phosphate (S3P) and phospho*enol*pyruvate (PEP). Upon extended incubation, it forms EPSP ketal by intramolecular nucleophilic attack of O4H on C2' of the *enol*pyruvyl group. EPSP ketal was previously proposed to form by non-enzymatic breakdown of the tetrahedral intermediate (THI) which had dissociated from AroA. In this study, EPSP ketal formed in the presence of excess AroA, which demonstrated that it was formed in the active site. This eliminated non-enzymatic THI breakdown as its source, and demonstrated that AroA forms either a discrete EPSP cationic intermediate, or a transition state with high cationic character. The pH dependence of non-enzymatic EPSP hydrolysis was examined in order to understand the intrinsic reactivity of the *enol*pyruvyl group. Acid catalysis accelerated EPSP hydrolysis $> 10^8$ -fold. These results provide evidence for *enol*pyruvyl activation through protonation at C3', forming an unstable cationic intermediate, or a highly cation-like transition state. The incorporation of ^2H into EPSP from solvent $^2\text{H}_2\text{O}$ during AroA-catalyzed hydrolysis was much slower than the hydrolysis rate, in the absence of inorganic phosphate in the reaction. This demonstrated that KIEs on AroA-catalyzed EPSP hydrolysis, when they are measured in the future, will reflect protonation of EPSP. A method was developed for KIE measurements on acid-catalyzed EPSP hydrolysis, which showed good reproducibility and no buffer dependence. Further experiments

need to be completed on the acid-catalyzed KIEs and enzyme-catalyzed KIEs, followed by transition state analysis. This will precisely define the transition state structure of the enzyme-catalyzed EPSP hydrolysis reaction, and provide a good starting point for designing AroA inhibitors.

Acknowledgements

I would like to thank my supervisor, Dr. Paul J. Berti, for giving me the opportunity to work in his lab, and for his guidance throughout this project. To my committee members, Dr. Graham McGibbon and Dr. Gerard D. Wright, thank you for your feedback and critiques along the way. I would like to thank Dr. Kirk Green and the staff at the McMaster Regional Centre for Mass Spectrometry for all their assistance with the mass spectrometer, and Dr. Donald Hughes for his help with NMR experiments. I need to also thank Dr. Shehadah Mized for his contribution to the EPSP ketal project, as well as Joan Lowe-Ching for her help with the pH profile of EPSP acid-catalyzed hydrolysis.

I want to thank the people at McMaster who have provided me with a wealth of knowledge and unending emotional support during my time in graduate school. To Menat Attia, Dr. Paul Loncke, Dr. Joe A. B. McCann, Amanda Ramnarine, and Fuzhong Zhang, this journey would not have been the same, or even possible, without any of you.

Finally, I need to thank my family for their constant encouragement. You all asked questions, even though you knew you wouldn't understand the answers. Thank you for always taking the time, and for listening. And to my future husband Sean, all I can say, is thank you for everything.

Table of Contents

| | |
|--|--------------------|
| <u>Abstract</u> | <u>iii</u> |
| <u>Acknowledgements</u> | <u>v</u> |
| <u>Table of Contents</u> | <u>vi</u> |
| <u>List of Abbreviations</u> | <u>viii</u> |
| <u>List of Figures</u> | <u>ix</u> |
| <u>List of Tables</u> | <u>xi</u> |
| <u>List of Tables</u> | <u>xi</u> |
| <u>Introduction</u> | <u>1</u> |
| Enzyme of Interest - AroA..... | 2 |
| Enzyme-Catalyzed Reaction..... | 2 |
| Proposed Mechanism | 3 |
| EPSP Ketal – A Mechanistically Relevant Side Product..... | 6 |
| X-ray Crystal Structure..... | 7 |
| Catalytic Residues in the Active Site..... | 10 |
| Inhibitors of AroA | 12 |
| Enzymes and Transition State Theory..... | 14 |
| Enzymes and Reaction Mechanism..... | 15 |
| Kinetic Isotope Effects | 17 |
| The Meaning of KIEs | 18 |
| Methods to Measure KIEs..... | 20 |
| Objective of Study..... | 21 |
| <u>Methods</u> | <u>22</u> |
| General | 22 |
| Protein Expression and Purification | 22 |
| Radiolabelled Small Molecule Synthesis and Purification..... | 23 |
| EPSP Ketal Formation with Excess AroA | 24 |

| | |
|--|------------------|
| Confirmation of EPSP Ketal Structure | 26 |
| Data analysis for EPSP Ketal Formation | 26 |
| Rate of ^2H incorporation and P_i Scavenging | 27 |
| Rate of AroA-catalyzed EPSP hydrolysis..... | 30 |
| Rate of Acid-catalyzed EPSP hydrolysis..... | 31 |
| Standard Curve on Mass Spectrometer..... | 32 |
| KIE by Mass Spectrometry | 33 |
| Synthesis of Radiolabelled EPSP | 34 |
| KIE by Radioactivity | 35 |
| <u>Results</u> | <u>38</u> |
| EPSP Ketal Formation with Excess AroA | 38 |
| Confirmation of EPSP Ketal Structure | 40 |
| Acid-catalyzed EPSP hydrolysis | 47 |
| Rate of ^2H incorporation..... | 48 |
| P_i Scavenging | 49 |
| Standard Curve on Mass Spectrometer..... | 54 |
| KIE by Mass Spectrometry | 55 |
| KIE by Liquid Scintillation Counting | 56 |
| <u>Discussion</u> | <u>58</u> |
| EPSP Ketal formation | 58 |
| Nucleophile vs. Electrophile Activation | 59 |
| Catalytic Advantage of Acid Catalysis..... | 60 |
| Energetic cost of EPSP cation formation | 62 |
| ^2H Incorporation | 62 |
| KIE interpretations | 63 |
| <u>Conclusions and Future Work</u> | <u>70</u> |
| <u>References</u> | <u>72</u> |

List of Abbreviations

| | |
|------------------|--|
| AroA - | <i>Eno</i> lpyruvyl Shikimate 3-phosphate synthase; |
| AroK - | Shikimate Kinase; |
| EPSP - | <i>Eno</i> lpyruvyl Shikimate 3-Phosphate; |
| IPTG - | isopropyl-beta-D-thiogalactopyranoside; |
| KIE - | Kinetic Isotope Effect; |
| MS - | Mass Spectrometer; |
| MurA - | UDP-N-Acetylglucosamine <i>eno</i> lpyruvyl transferase; |
| NMR - | Nuclear Magnetic Resonance; |
| PEP - | Phospho <i>eno</i> lpyruvate; |
| PPDK - | Pyruvate phosphate dikinase; |
| PPiase - | Inorganic pyrophosphatase; |
| P _i - | Inorganic phosphate; |
| S3P - | Shikimate 3-Phosphate; |
| THI - | Tetrahedral Intermediate; |
| TS - | Transition State; |

List of Figures

| | |
|---|----|
| Figure 1. Carboxyvinyl transfer by AroA and MurA. | 3 |
| Figure 2. The three proposed acid/base catalytic residues. | 11 |
| Figure 3. Reaction Space diagram..... | 17 |
| Figure 4. The origin of isotope effects. | 19 |
| Figure 5. ³³ P Chromatogram. | 25 |
| Figure 6. P _i scavenging methods. | 29 |
| Figure 7. Radioactivity Chromatogram..... | 36 |
| Figure 8. Kinetic Mechanism for EPSP ketal formation..... | 38 |
| Figure 9. Reaction profiles for EPSP ketal formation under different conditions. | 40 |
| Figure 10. ¹ H spectra of EPSP ketal | 43 |
| Figure 11. ¹³ C spectrum of EPSP ketal. | 44 |
| Figure 12. Gradient Proton COSY 2-D NMR spectrum of EPSP ketal. | 45 |
| Figure 13. ¹ H- ¹³ C: Gradient HSQC spectrum of EPSP ketal..... | 46 |
| Figure 14. pH profile of Acid-Catalyzed EPSP Hydrolysis..... | 48 |
| Figure 15. Mechanism of ² H incorporation. | 50 |
| Figure 16. Measurement of ² H incorporation..... | 51 |
| Figure 17. Controls for ² H incorporation..... | 52 |
| Figure 18. P _i Scavenging experiments..... | 53 |
| Figure 19. Standard curve on mass spectrometer. | 55 |
| Figure 20. Fate of the EPSP Cation. | 60 |
| Figure 21. Reaction Space diagram of the initial steps of the AroA-catalyzed reaction..... | 64 |

| | |
|---|----|
| Figure 22. Reaction coordinate of AroA-catalyzed EPSP hydrolysis..... | 65 |
| Figure 23. Summary of KIE results. | 66 |
| Figure 24. Reaction coordinate of Acid-catalyzed EPSP hydrolysis..... | 68 |

List of Tables

| | |
|---|----|
| Table 1. Rates of EPSP ketal formation and EPSP hydrolysis..... | 39 |
| Table 2. Chemical shifts and coupling constants for EPSP ketal, shikimate 3-phosphate, and shikimic acid. | 41 |
| Table 3. AroA-Catalyzed ^2H incorporation versus EPSP Hydrolysis. | 54 |
| Table 4. $[3\text{-}^{13}\text{C}]$ EPSP KIEs for acid catalyzed EPSP hydrolysis measured by mass spectrometry. | 56 |
| Table 5. $[1\text{-}^{14}\text{C}]$ EPSP KIEs for acid-catalyzed EPSP hydrolysis. | 57 |
| Table 6. $[2\text{-}^{14}\text{C}]$ EPSP KIEs for acid-catalyzed EPSP hydrolysis. | 57 |
| Table 7. $[3\text{-}^{14}\text{C}]$ EPSP KIEs for acid-catalyzed EPSP hydrolysis. | 57 |

Introduction

Enzymes are an important class of targets for novel drug development (1). It is possible to design inhibitors which bind to the enzyme active site as mimics of the transition states or high energy intermediates of the enzyme-catalyzed reaction. These are effective inhibitors because if the enzyme mutates to decrease its binding affinity towards the inhibitor, it will also lose affinity for its natural substrate. It is therefore difficult for organisms to become resistant to these types of inhibitors. There are many pathogenic organisms, such as *Mycobacterium tuberculosis*, which are known for their resistance to multiple drugs (2). To continue to effectively treat bacterial infections which are prone to resistance, there is a constant demand for new antibiotic development.

The enzyme AroA (*enol*/pyruvyl shikimate 3-phosphate synthase) is actively being studied as a potential target for inhibitor design. It catalyzes the sixth step in the shikimate pathway (3), which is found in all plants and bacteria (4), and some parasites (5). As this pathway is not found in humans, it makes an attractive target for novel drug development. The pathway leads to the synthesis of aromatic compounds in these species, such as aromatic amino acids, and has been shown to be an essential pathway in *M. tuberculosis* (6). The most current research focuses on understanding the nature of the molecules this enzyme stabilizes, including the transition state structure, in order to design good

inhibitors and better drugs to treat this disease. The following thesis describes a mechanistic investigation of AroA.

Enzyme of Interest - AroA

The chemistry of the reaction catalyzed by AroA is unusual. It is one of only two enzymes that catalyze carboxyvinyl transfer (Figure 1). The other is MurA, an enzyme found in the peptidoglycan synthesis pathway. The chemistry and mechanism of AroA have been well established and reviewed (7). Several crystal structures have been determined, with the protein alone (8), and in the presence of substrates, products, and intermediates of the reaction, including some inhibitors (9-11).

Enzyme-Catalyzed Reaction

AroA catalyzes a simple addition-elimination mechanism (Figure 1). In the addition step, C3 of phosphoenolpyruvate (PEP) is protonated to form a methyl group, combined with nucleophilic attack at C2 by the O5H group on shikimate 3-phosphate (S3P) to form the tetrahedral intermediate (THI). In the elimination step, phosphate is eliminated through C-O bond cleavage to form enolpyruvyl shikimate 3-phosphate (EPSP).

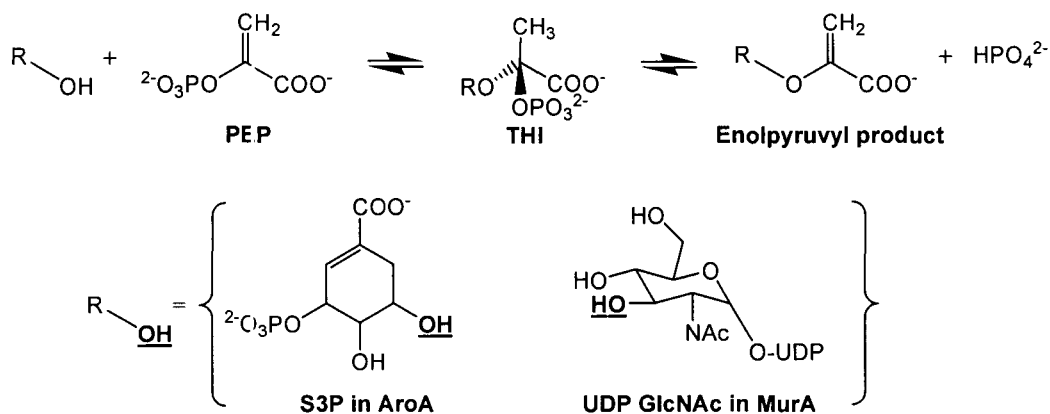


Figure 1. Carboxyvinyl transfer by AroA and MurA.

Proposed Mechanism

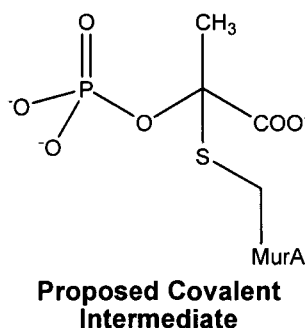
The pre-steady state kinetic parameters of the AroA reaction have been determined (7). The mechanism was proposed to be ordered, with S3P binding first, followed by PEP, and phosphate released first, followed by EPSP. Further steady-state kinetic data showed that the binding of substrates is actually random in the forward (12) and reverse reactions (13). Recent X-ray crystallography data of the *Streptococcus pneumoniae* AroA showed that the residues in the S3P binding pocket are all located on the N-terminal domain of the protein, while the residues that make contacts with PEP are found on both the N- and C-terminal domains (11). This would again suggest an ordered binding, with S3P binding first, causing a conformational change which brings the two domains of the protein together, and revealing the PEP binding pocket.

The reaction stereochemistry is an important question. It has been shown that the addition and elimination steps occur with opposite relative stereochemistry, that is, either *syn/anti* or *anti/syn* (14). The absolute

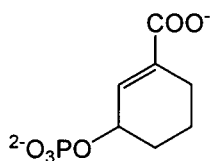
stereochemistry shows that AroA catalyzes the 2-*si* face addition of hydrogen to C3 of PEP (15), which is a similar result to the absolute stereochemistry of MurA (16). With this result, the relative stereochemistry would have to follow *anti* addition, followed by *syn* elimination (17).

Previously, there were two proposed reaction pathways: (i) the enzyme was acting as the nucleophile to form a covalently bound enzyme intermediate, or (ii) a single intermediate with S3P acting as a nucleophile.

Evidence for a covalently bound enzyme intermediate came from MurA, the other carboxyvinyl transferase (18). When radioactive substrates were used, both in the forward and reverse reactions, some radioactivity would remain on the enzyme, even after protein denaturation. The covalent intermediate involved the PEP portion of the substrate, and was hypothesized to form through the nucleophilic attack of a reactive cysteine at C2 of PEP. It was found, once this protein was overexpressed at high levels in *E. coli*, that it co-purified with 1 equivalent of PEP covalently attached to the enzyme (19). This supported a mechanism involving a covalent phospholactoyl intermediate.



A similar mechanism was also proposed for AroA. Because of the similarity of the two enzymatic reactions, it was thought that AroA would follow a similar mechanism (14, 20). Some of the evidence for this mechanism in AroA included the observation that the hydrogen atoms on C3 of PEP were exchanged in the presence of dideoxy-S3P, a substrate which lacks the nucleophilic hydroxyl group (20), as well as the presence of what was thought to be such an intermediate in ^{13}C NMR studies (21). This was later shown to be EPSP ketal, a side product of the AroA-catalyzed reaction, which will be discussed further in this report.



Dideoxy-S3P

The second, and currently accepted, mechanism was formation of a non-covalent tetrahedral intermediate (22, 23) (Figure 1). The THI was trapped, purified and its structure elucidated (24). It was then characterized to be a true intermediate of this reaction by showing that THI formation and enzymatic breakdown were fast enough to be catalytically relevant; that is, it is kinetically competent (25). The THI had a half-life of 45 min at pH 7, more than 48 hours at pH >7 (26) and 24 days at pH 12 (27). Because of its stability at high pH, this intermediate was amenable to further kinetic study. ^{13}C NMR studies were carried out and showed the THI bound in the enzyme active site, with no other intermediates formed (28).

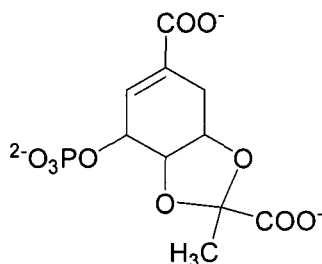
With strong evidence for the THI mechanism in AroA, and the similarities between these two enzyme reactions, the question was raised again whether MurA did in fact follow the covalently-bound intermediate mechanism. A non-covalent THI was isolated and characterized (29), however, both this intermediate and the covalently-bound intermediate could be isolated from the same reaction (30).

In attempts to determine which of these intermediates was part of the preferred catalytic mechanism, site directed mutagenesis was performed at the proposed catalytic site of Cys115 (31). This residue was proposed to be the thiolate group acting as the enzyme nucleophile. The residue was mutated to Asp and to Glu, which both have carboxylate side chains that are not as reactive as the thiolate group of Cys. Both these mutants were still active, however they were resistant to the activity of fosfomicin. This provided evidence that the formation of the covalent intermediate is not required for the MurA reaction.

EPSP Ketal – A Mechanistically Relevant Side Product

After the THI had been identified and kinetically characterized, a side product was isolated and identified as EPSP ketal (32). This product forms through the intramolecular nucleophilic attack of the O4H group on C2 of PEP at a rate of $3.3 \times 10^{-5} \text{ s}^{-1}$ (28), a rate too slow for EPSP ketal to be an intermediate of the reaction. It was originally proposed to form through non-enzymatic breakdown of the THI. Our group has studied the non-enzymatic breakdown of THI and found that too little EPSP ketal is formed under these conditions to

account for its formation in the presence of AroA (27). The formation of this side product can be used as a tool to help understand the AroA mechanism.



EPSP ketal

Testing for EPSP ketal formation in reactions where AroA is present in excess over substrates would eliminate any non-enzymatic source of THI breakdown. If EPSP ketal forms under these conditions, this would indicate that it is formed in the active site of AroA. This is one of the primary investigations of this study.

X-ray Crystal Structure

The crystal structure for free AroA in an open conformation was solved at 3Å resolution (8). Due to the low resolution, the peptide backbone could be traced, but not the amino acid side chains. This structure showed AroA to be a single polypeptide chain that folds into two distinct domains connected through two peptide crossovers. The domains are similar in structure with each having three repeating folding units of four-stranded β -sheets and two α -helices in a $\beta\alpha\beta\alpha\beta\beta$ pattern.

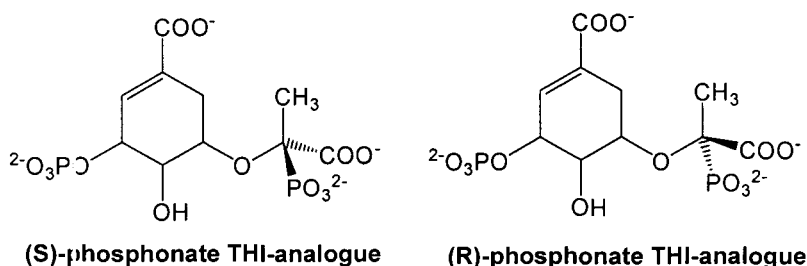
MurA and AroA are homologues, even though they have only 18% sequence identity. The structure of *E. coli* MurA has been solved in the open,

substrate-free conformation (33), and with UDP-GlcNAc and fosfomycin bound (34). These structures were solved to 2.0Å and 1.8Å respectively. MurA also consists of two a domain structure, with the same folding pattern as AroA (33). The similarities in structural features are what allow for the similar chemistry to be catalyzed, even with the minimal sequence identity.

Other AroA structures have since been solved, with S3P, as well as with S3P and glyphosate, an AroA inhibitor, at resolutions of 1.6Å and 1.5Å, respectively (9). With S3P bound, AroA was in a closed conformation, with the two domains closer together. This closed structure also defined the location of the active site and identified residues close enough to interact with S3P. Residues involved in contacts with PEP could be hypothesized, based on the assumption that glyphosate was binding in the same manner as PEP.

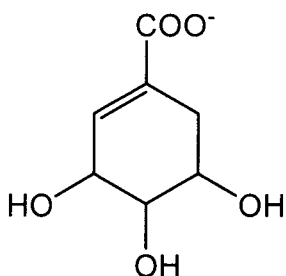
A tool used to probe some of AroA's conformational changes is the intrinsic tryptophan fluorescence. There is a Trp residue within the enzyme active site, and the binding of substrates, including EPSP and [S3P + glyphosate], leads to a decrease in fluorescence. In a study of AroA using phosphate analogues, a binding pocket for both EPSP and P_i was demonstrated (35). Using AroA_D313A, a mutant with very low activity (36), there were two distinct changes in tryptophan fluorescence, first upon binding of EPSP, followed by either phosphate or arsenate. This suggests the enzyme under goes two separate conformational changes.

Further evidence for conformational flexibility comes from the X-ray crystal structures of AroA complexed with phosphonate analogues of the THI (10). One would expect that the (S)- phosphonate THI analogue would be the better inhibitor, as this corresponds to the correct configuration of the THI (37, 38). However, the (R)-phosphonate analogue is the more potent inhibitor ($K_{iS3P} = 16 \text{ nM}$ vs. 750 nM for the (S)-phosphonate analogue). (R)-phosphonate appears to cause a greater conformational change in some of the strictly conserved residues in the enzyme active site, Arg124 and Glu341.



The most recent AroA crystal structure examined the structure of AroA bound to shikimate, as opposed to the natural substrate S3P, and glyphosate (39). AroA will bind to shikimate, which contains a hydroxyl group instead of the 3-phosphate group in S3P; however the missing ionic interactions lead to changes in the glyphosate/PEP binding pocket. While the conformational change in the enzyme is small, there is a significant decrease in glyphosate sensitivity. With shikimate as a substrate, there is an increase in IC_{50} by a factor of > 250 (39). This result again suggests that the enzyme active site is flexible, as it can accommodate a variety of substrates. The changes to the active site upon binding of these pseudosubstrates, however leads to a less catalytically efficient

enzyme. This will be an important consideration when designing inhibitors for AroA.



Shikimate

The X-ray crystallography data suggests that there are several important contacts that the substrates make with the enzyme. With the mechanistic and crystallography data, the residues directly involved in catalysis are still subject to debate. The crystal structures identified the amino acids present in the active site; however identifying function requires functional characterization of mutant AroAs.

Catalytic Residues in the Active Site

There has been some controversy as to which amino acids are involved in catalysis (Figure 3). Three groups recently published work identifying the amino acid residues important for catalysis.

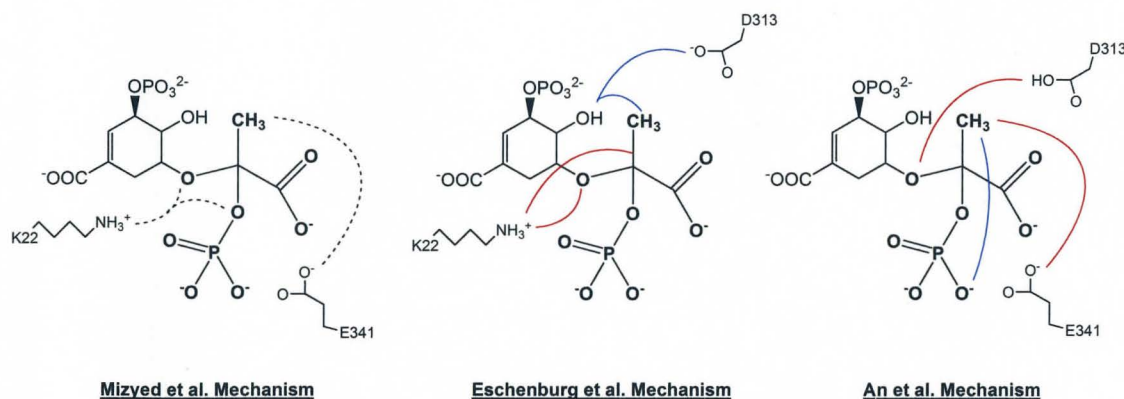


Figure 2. The three proposed acid/base catalytic residues.

Each mechanism is shown after the formation of the THI. Red lines indicate interactions in the addition step, blue lines indicate interactions in the elimination step, and dashed lines indicate interactions in both steps. The residues are shown in their protonation states after the addition step.

Our group has proposed that the same residues act as general acid/base catalysts in the forward and reverse reaction of the AroA mechanism. This was due to the observation that no residue was found to be important for only one step of the reaction, i.e., either addition or elimination, without being important for the other step (36). In the addition step, the residues that we proposed are Lys22 as a general base and Glu341 as the general acid. In the elimination step, the roles would be reversed, with Lys22 serving as general acid and Glu341 as general base. This reaction would then follow the stereochemistry of *anti* addition with *syn* elimination, as previously proposed (17).

Eschenburg et al. agreed that Lys22 is involved in the addition step, however they proposed that it is both the general acid and general base. In the elimination step, they proposed that Asp313 acts as a general base through an intramolecular proton transfer (37). This mechanism disagrees with the proposed

stereochemistry from the literature in that it would involve *syn* addition followed by *anti* elimination.

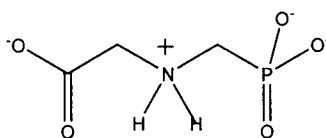
An et al. proposed a different set of residues as well (38). They agreed with our mechanism that Glu341 is acting as a general acid in the addition step, however they believed that it is Asp313 acting as the general base. They proposed that the elimination step occurs with the phosphate leaving group acting as the general base in an intramolecular elimination. This mechanism would follow the accepted *anti* addition followed by *syn* elimination.

This controversy must be addressed. It is important to know how the enzyme is catalyzing its reaction, to better understand how to effectively inhibit it.

Inhibitors of AroA

As AroA is a target for the development of novel antimicrobials, much of the current research is focused on trying to find new inhibitors. There is already a commercially relevant inhibitor, glyphosate (*N*-(phosphonomethyl)glycine) (40). It is the active ingredient in the herbicide Roundup™; however it is not active as an antibiotic. Presumably, this is due to the highly charged nature of the molecule, which would make it difficult to cross the bacterial outer membrane. Glyphosate inhibits AroA reversibly by binding to the enzyme•S3P complex (41). It is a competitive inhibitor of PEP, and an uncompetitive inhibitor with respect to S3P (20). In the reverse reaction, glyphosate inhibition is non-competitive with respect to P_i (42) and uncompetitive with respect to EPSP (43). It was thought

that glyphosate was a transition state analogue, mimicking the presumed cationic intermediate character of the addition step transition state (42). This was initially thought to be unusual, since glyphosate does not inhibit any other PEP-utilizing enzyme, not even MurA. However, it was later shown that glyphosate could inhibit AroA in the presence of EPSP, demonstrating that glyphosate does not occupy the same position in the AroA active site as the *enol*/pyruvyl portion of EPSP, which it should do if it is a transition state mimic (43). Glyphosate is effective as a herbicide, but the search continues for a novel AroA inhibitor which could act as an effective antimicrobial.



Glyphosate

As several PEP-utilizing enzymes could be potential antimicrobial targets, there have been attempts to create a PEP analogue which could act as an effective inhibitor for all these enzymes. Many modifications of the PEP structure have been made, including halogenation of the methylene group, and varying both the carboxylate and the phosphate functional groups (44). The most potent inhibitors for several PEP-utilizing enzymes are those containing modifications at the vinyl protons. (Z)-3-fluoro-PEP has been a useful tool in assigning the stereochemistry of the AroA reaction (15).

Another approach has been to seek synthetic analogues that specifically inhibit AroA, rather than a general inhibitor of all PEP-utilizing enzymes (45) and

some of these have been found to be quite potent. Two phosphonate THI-analogues, the (R)- and (S)- diastereomers, are competitive inhibitors with K_i 's against S3P of 16 nM and 750 nM (10) and K_i 's against EPSP of 15 nM and 1130 nM (46), respectively.

Many potential inhibitors have been tested; however a successful antimicrobial still does not exist for this enzyme. The implications of these studies demonstrate that a more rational method of inhibitor design is needed in order to find a potent inhibitor. Two methods for this purpose have been used in this study: (i) trying to understand high energy intermediates which may exist along the reaction coordinate pathway, such as the precursor to EPSP ketal and (ii) solving the transition state structure of either the addition or elimination step of the reaction.

Enzymes and Transition State Theory

The transition state (TS) is the highest energy point on the reaction coordinate, and is important because enzymes increase reaction rates by decreasing the TS energy (47). TS theory states that enzymes bind to the TS more tightly than either substrates or products. Therefore, designing an inhibitor which mimics the structure of the TS should create a tight binding inhibitor.

A TS inhibitor of AroA would have similar properties to the THI-analogues discussed earlier, namely, functional groups correctly placed in the enzyme active site, to induce a conformational change of the enzyme into the closed

position. The challenge will be to mimic the correct charge on these functional groups, as highly charged inhibitors, including glyphosate, cannot act as antibiotics. Presumably the highly charged nature of these inhibitors prevents them from entering the cell as they cannot diffuse across the bacterial outer membrane. In studies of AroA with phosphate analogues, it was shown that P_i could activate the *enol*/pyruvyl group (35). It may be possible to design a TS mimic which lacks the phosphate group, and exploit the high intracellular concentration of P_i , which is 20 mM in *E. coli* (48). This would reduce the challenge of transporting a highly charged inhibitor with a P_i functional group across the cell membrane.

Enzymes and Reaction Mechanism

Before determining the TS of a reaction, it is important to first understand the reaction mechanism being studied. A familiar method to describe enzyme and chemical substitution reactions is the Ingold system using S_N1 and S_N2 . S_N1 describes a 2 step mechanism where a leaving group departs to form a discrete intermediate, followed by nucleophile attack. An S_N2 mechanism describes a mechanism, whereby nucleophile attack and leaving group departure occur in a more concerted fashion. This method can be limiting to describe reactions as it does not provide mechanistic information, for example, as to the synchronicity of an S_N2 reaction.

The IUPAC method provides information about the mechanism while describing the reaction (49). This method describes individual steps in a reaction

as being associative (A) or dissociative (D). For example, a synchronous S_N2 reaction would be described as $A_N D_N$, with the association of the nucleophile (subscript N) concerted with the departure of the leaving group. An S_N1 reaction would be described as $D_N + A_N$, as there are 2 steps in the reaction, and a stable intermediate is formed between these 2 steps as denoted by '+'. A non-synchronous S_N2 mechanism, can be described as $D_N^* A_N$, with departure of the leaving group occurring in advance of nucleophile approach. The '+' in the previous example indicates that the intermediates are sufficiently long lived to separate by diffusion, while the '*' indicates that the intermediates do not dissociate and are short lived. The synchronicity of a reaction can be seen in More O'Farrell – Jencks reaction diagram (Figure 3). This is a useful method used to describe different reactions and will be used in further discussions of the AroA reaction.

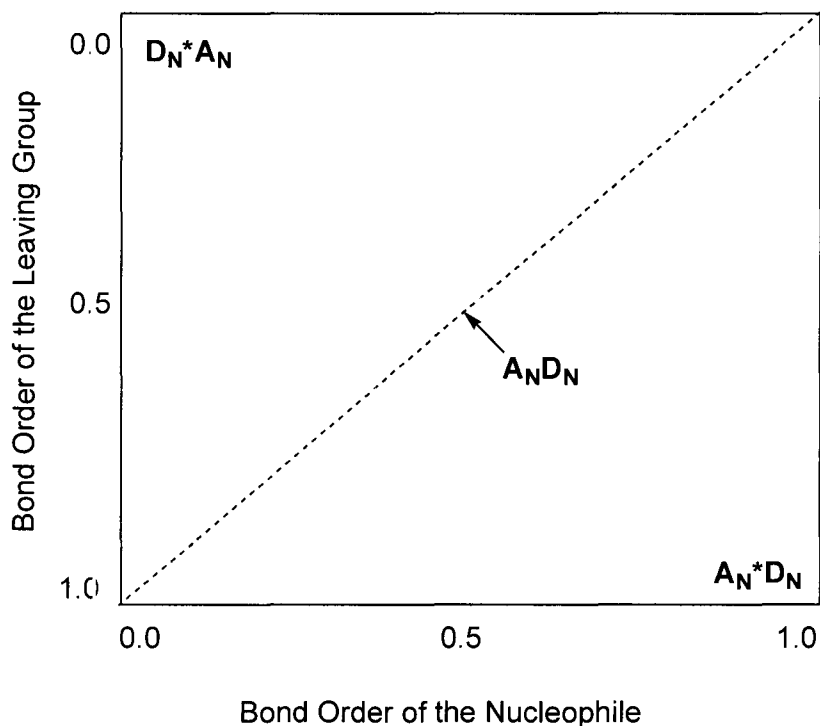


Figure 3. Reaction Space diagram.

Kinetic Isotope Effects

A tool used in our lab to understand transition states and enzyme mechanisms is kinetic isotope effect (KIE) measurements (50). KIEs provide information about the bonds which are broken and formed as substrates approach the TS in a reaction. The vibrational environment of the atoms will change as bonds break and new bonds form between the reactants and the TS. Although TSs exist for a vanishingly small amount of time, the change in the vibrational environment can be measured using isotopically labelled compounds. 'Heavy' labelled isotopes, such as ^2H or ^3H , will react at different rates than their 'light' counterparts, ^1H . The reactant can be labelled at various positions; those

which will undergo a change in bonding (a primary KIE) as well as those which do not have any bonds broken or formed (a secondary KIE).

A KIE is defined as the ratio of rate constants of the light and heavy isotopes, i.e., $KIE = k^{light}/k^{heavy}$ (51). If the light isotope reacts faster, this will result in a $KIE > 1$, known as a 'normal' KIE. If the heavy isotope reacts faster, this leads to a $KIE < 1$, known as an 'inverse' KIE. If an atom has a normal KIE, then the atom is moving into a looser vibrational environment at the TS. This could mean that there is less bond order around that atom, or that there is more relative movement around that atom at the TS. For an inverse KIE, the opposite is true; the atom is moving into a tighter vibrational environment. This can provide information about the nature of the reaction, such as whether it follows a step-wise or a concerted mechanism.

The Meaning of KIEs

There are three factors which contribute to KIEs, the change in mass and moment of inertia (MMI), zero point energy (ZPE) and excited state energy (EXC). These contributions can be expressed in the following equation:

$$KIE = MMI * ZPE * EXC$$

As the labelled molecules in the KIE reactions are atoms with increased mass, there will be a decrease in the overall motion of the molecule, which gives rise to MMI. Some of the molecules in the reactant are vibrationally excited,

which contributes to EXC. The greatest contribution to the KIE measurement comes from ZPE.

When there is an isotopic substitution in a molecule, there is a change in the zero point energy, or the vibrational energy of the molecule at 0 K. As bonds become weaker at the TS, ZPEs decrease, and they decrease more for light atoms, and this results in a normal KIE (Figure 4a). If the bonds become tighter at the TS, there will be a greater decrease in the activation energy of the heavy atom, leading to an inverse isotope effect (Figure 4b)

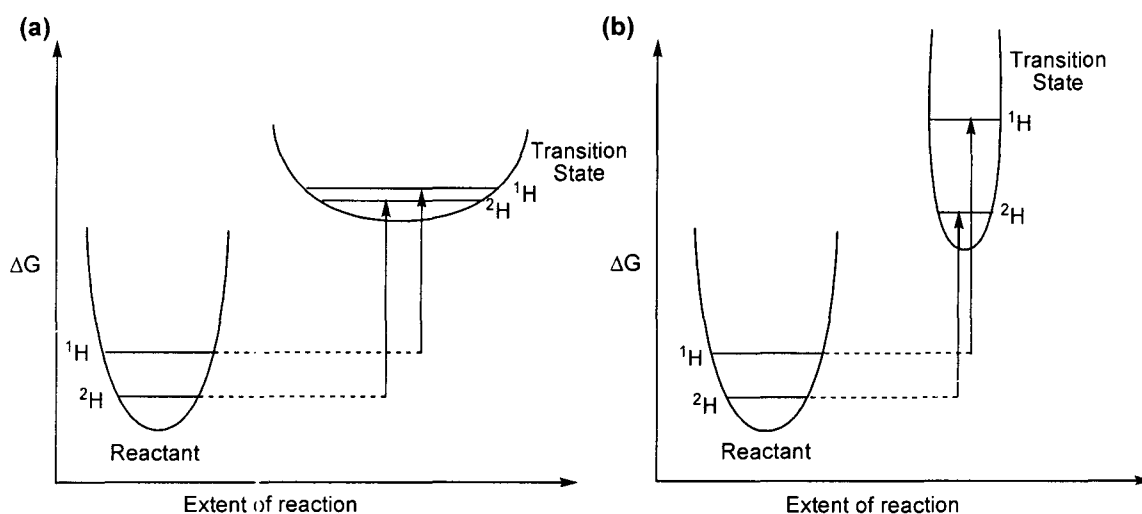


Figure 4. The origin of isotope effects.

Demonstration of the change in the ZPE as a molecule goes from reactant to TS. (a) Normal isotope effect. The light isotope has a smaller change in activation energy and therefore the heavy isotope which must overcome a greater energy barrier to get to the TS. (b) Inverse isotope effect. The heavy molecule has a lower energy barrier to overcome to reach the TS.

Methods to Measure KIEs

KIEs can be measured either competitively or non-competitively (52). In the competitive method, a mixture of the light and heavy isotopically labelled molecules is made, and the difference in relative rates between the light and heavy isotopes is determined. The different isotopes will be competitive substrates and therefore if there is a KIE, they will have different k_{cat}/K_M values. In the non-competitive method, the light and heavy isotopes are reacted separately, and the difference in their rates measured. With this method it is possible to determine KIEs on all kinetic parameters, k_{cat} , K_M , and k_{cat}/K_M .

There are several technologies which can be used to measure KIEs. The most commonly used method is liquid scintillation counting, using radioactive substrates, commonly ^3H and ^{14}C (52). Recently, a method using ^{33}P and ^{32}P was described (53). The importance of radioisotope selection is that if the energies of the β -particles emitted are different, it is possible to distinguish the two isotopes in one solution. It is also possible to measure KIEs by isotope ratio mass spectrometry (54). This method provides very precise results, but similar to using radiolabels, can be limited by the ability to synthesize the labeled substrate. In order to avoid this labeling problem, a method was recently developed to measure KIEs by NMR using ^{13}C natural abundance ratios for the methyl glucoside hydrolysis reaction (55). While this method provides the advantage of eliminating the need for remote labeling, it does require a large amount of starting material.

It is important to measure KIEs for both enzymatic and non-enzymatic reactions, so that the change in TS between enzymatic and non-enzymatic reactions can be defined. This is important in order to understand explicitly what the enzyme is doing to lower the activation energy of the TS. It is also necessary to know specifically which chemical step is being probed. One of the challenges in studying the AroA reaction is that it is a two step reaction. With two steps in the reaction, there are potentially two TS structures to be solved.

Objective of Study

This project began with a study of EPSP ketal formation in the presence of excess AroA. The goal was to measure the rate of EPSP ketal formation, under conditions of excess enzyme, and to eliminate any non-enzymatic source. Over the course of these studies, conditions were established to measure KIEs on the enzyme-catalyzed EPSP hydrolysis reaction. A method was established to measure KIEs of the acid-catalyzed EPSP hydrolysis reaction. The EPSP ketal results, in combination with the KIE results, will provide information about the mechanism of AroA, and the nature of the TS. By determining the TS structure, this provides important information which can be used to design a TS mimic, which could further be tested as a novel antimicrobial against this enzyme.

Methods

General

Reagents were purchased from Sigma/Aldrich or Bioshop Canada, unless otherwise noted. [γ - ^{33}P]ATP, [γ - ^{32}P]ATP, and [1- ^{14}C]pyruvate were from Amersham/GE Healthcare. [2- ^{14}C]pyruvate and [3- ^{14}C]pyruvate was from American Radiolabelled Chemical. [3- ^{13}C]pyruvate and $^2\text{H}_2\text{O}$ were purchased from Cambridge Isotopes Labs.

Protein Expression and Purification

E. coli AroA containing a C-terminal His₆ tag was prepared previously (36). The expression vector was transformed into BL21*(DE3) cells by electroporation, and the reaction was plated onto LB agar + 50 $\mu\text{g}/\text{mL}$ kanamycin, and incubated overnight at 37 °C. A colony was then selected to inoculate LB media + 50 $\mu\text{g}/\text{mL}$ kanamycin, which was left at 37 °C overnight, with shaking. The next day, the overnight culture was diluted 40-fold into 6 to 9 L of fresh LB + 50 $\mu\text{g}/\text{mL}$ kanamycin. The OD₆₀₀ of the diluted culture was monitored, and upon reaching 0.6, 1 mM IPTG was added. The culture was incubated for 4 hours at 37 °C with shaking. The cells were centrifuged at 5000 \times g for 10 min and the pellet was suspended in 25 mL of lysis buffer (50 mM Tris-HCl pH 7.5, 300 mM NaCl and 20 mM imidazole) per litre of culture.

Cells were lysed using an EmulsiFlex® -C5 High Pressure homogenizer (Avestin, Inc.), doing three passes at 10,000 psi, until the lysate was cleared. The cellular debris was centrifuged at 20,000 × g, and the supernatant was applied to a Ni⁺⁺ affinity column (Chelating Sepharose™ Fast Flow, Amersham). The non-specific proteins were washed from the column using lysis buffer, after which AroA was eluted with 50 mM Tris-HCl pH 7.5, 300mM NaCl, and 500 mM imidazole. The protein was exchanged into storage buffer (50 mM Hepes, pH 7, and 50 mM KCl) and concentrated in a Amicon stirred cell (Millipore, Corp) over a 10 kDa cutoff membrane (YM10 ultrafiltration membrane, Millipore, Corp).

As experiments required an active enzyme concentration of 1 mM, it was essential to know both the total and active protein concentrations. The total protein concentration was determined from A_{280} using $\epsilon_{280} = 3.55 \times 10^4 \text{ M}^{-1} \text{ cm}^{-1}$ as determined previously (56). The active AroA concentration was determined by fluorescence titration of 0.5 μM AroA with S3P in the presence of 250 μM glyphosate (36, 43, 57). Typically, active AroA was ~45% of the total protein concentration, consistent with our previous findings (36), and similar to a previous study where glyphosate binding to AroA•EPSP had a stoichiometry of ~63% (57).

Radiolabelled Small Molecule Synthesis and Purification

Shikimate 3-phosphate (S3P) and [³³P]S3P were prepared in a 100 μL reaction containing 50 mM Hepes pH 7, 50 mM KCl, 10 mM MgCl₂, 100 mM shikimic acid, 50 mM PEP, 1 mM ATP (25 μCi of [γ -³³P]ATP), 25 mM sodium tungstate, 60 U pyruvate kinase/mL reaction and 100 μL of shikimate kinase/mL

reaction. Purification was performed using a Mono Q ion exchange column and elution with 50 mM to 800 mM ammonium formate, pH 8.0, over a 30 min gradient at 0.5 mL/min, and A_{240} detection (36). Under these conditions, S3P cleanly eluted at 19 min.

$[^{33}\text{P}]$ EPSP was prepared from $[^{33}\text{P}]$ S3P in a 1 mL reaction containing 50 mM Tris-HCl, pH 7.5, 0.5 μM AroA, 150 μM $[^{33}\text{P}]$ S3P and 300 μM PEP. Purification was performed using a Mono Q ion exchange column with a gradient of 100 mM to 600 mM ammonium bicarbonate, pH 10.0, over a 30 min gradient at 0.5 mL/min, and A_{240} detection. EPSP cleanly eluted at 30 min.

EPSP Ketal Formation with Excess AroA

Reactions to detect EPSP ketal formation contained 600 or 750 μM $[^{33}\text{P}]$ S3P (0.7 or 0.9 μCi), 1.33 equivalents of active AroA, 50 mM HEPES, pH 7.0, 50 mM KCl, 5% glycerol, at 25 °C either in 100 or 250 μL reaction volumes. The reactions contained equimolar or 6.7 equivalents of PEP, with some of the 6.7 equivalents reactions also containing 10 mM potassium phosphate (P_i). AroA-catalyzed $[^{33}\text{P}]$ EPSP breakdown reactions were conducted with 750 μM $[^{33}\text{P}]$ EPSP (0.5 μCi), 1 mM active AroA in 100 μL of 50 mM HEPES, pH 7.0, 50 mM KCl, 5% glycerol, at 25 °C. Each aliquot was quenched with 0.2 M KOH to stop the reaction, and the protein was removed by centrifugal ultrafiltration over 10 kDa cutoff membranes (Microcon YM10, Millipore, Corp.). The reaction products were then separated by ion-paired C18 reverse phase HPLC (25 cm \times 4.6 mm, Supelcosil LC-18-T, 5 μm particles) with isocratic elution

in 100 mM KPi , pH 6.0, 4 mM $(\text{Bu}_4\text{N}^+)_2\text{SO}_4^-$ at 1 mL/min. ^{33}P was detected by flow scintillation analysis using a Packard 150T in-line flow scintillation analyzer, with Ultima-Flo AlP scintillation fluid (Packard) flowing at 4 mL/min, being mixed with the column eluate before entering the scintillation detector. The approximate elution times were: $[^{33}\text{P}]\text{S3P}$, 9.6 min, $[^{33}\text{P}]\text{EPSP ketal}$, 22.5 min, and $[^{33}\text{P}]\text{EPSP}$, 33.9 min, as seen in Figure 5. Concentrations of $[^{33}\text{P}]\text{S3P}$, $[^{33}\text{P}]\text{EPSP ketal}$, and $[^{33}\text{P}]\text{EPSP}$ were calculated from the ratios of peak areas from flow scintillation analysis and the known $[^{33}\text{P}]\text{S3P}$ concentration at the beginning of the reaction, or $[^{33}\text{P}]\text{EPSP}$ for hydrolysis reactions.

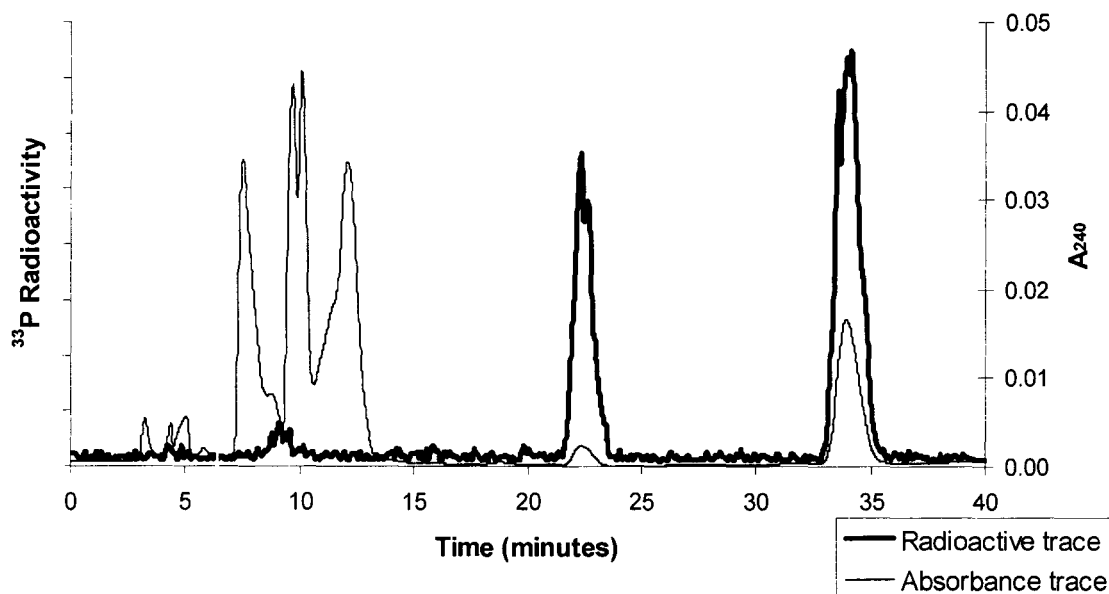


Figure 5. ^{33}P Chromatogram.

UV and ^{33}P chromatograms at $t = 8$ h. Elution of ^{33}P radioactivity at 9, 23 and 34 min corresponded to the elution times of standard S3P, EPSP ketal and EPSP, respectively.

No $[^{33}\text{P}]\text{THI}$ was observed in the experiments, as over the time required to remove the protein by ultrafiltration, THI was converted enzymatically to S3P and

EPSP. We showed previously that 0.2 M KOH is not sufficient to completely denature AroA_{H6}•THI (36).

Confirmation of EPSP Ketal Structure

Unlabeled EPSP ketal for NMR identification was prepared from unlabeled S3P under the same conditions from a 10 mL reaction mixture. EPSP ketal was dissolved in ²H₂O, after lyophilisation and spectra were recorded on a Bruker Avance 700 MHz NMR spectrometer. ¹H, and ¹³C NMR spectra were acquired, as well as 1D-TOCSY, COSY, HSQC and HMBC. These spectra were compared to shikimic acid and S3P standards, which were obtained on the Bruker 600 MHz NMR spectrometer.

Data analysis for EPSP Ketal Formation

The rates of formation/disappearance of EPSP ketal, S3P, and EPSP were analyzed by non-linear least squares fits to first order rate constants, and by numerical simulation. Fitting to first order rate constants was appropriate in certain conditions. Reactions with excess PEP and 10 mM P_i, or with EPSP only, were fitted to first order rate constants. The reactions with equimolar S3P and PEP, and with 6.7 equivalents of PEP would not necessarily be expected to fit first order rate constants because the proportion of E•EPSP•P_i would increase during the reaction. If $k_{+7a,b} > k_{+7c}$, EPSP ketal formation would accelerate as P_i accumulated, while it would slow if $k_{+7c} > k_{+7a,b}$. The fact that the progress curves appeared to follow first order progress curves implied that k_{+7a} to k_{+7c} were

broadly similar (see below). As a result, the values of k_{+7a} to k_{+7c} were eventually made equal to each other.

Numerical simulations used the AroA kinetic mechanism elucidated by Anderson and Johnson (58) under the same reaction conditions, except for the presence of 5% glycerol in the present study. Simulations were performed using KinTekSim, an implementation of KinSim and FitSim (59, 60). The microscopic rates constants k_{-1} to k_{-6} were fixed at the previously reported values (58), and the values of k_{+7a-c} and k_{+8} were fitted.

Rate of ^2H incorporation and P_i Scavenging

As a test for reversible EPSP cation formation, AroA-catalyzed EPSP hydrolysis was run in 50% $^2\text{H}_2\text{O}$. It was necessary to ensure that any ^2H exchange was due to EPSP cation formation, and not from THI formation due to P_i in the reaction. Any P_i present would be incorporated into the AroA reaction and lead to PEP formation. Three different reaction conditions were used to scavenge free P_i in solution. The first condition simply involved adding pyruvate kinase (PK) and ADP to the reaction. With PK and ADP in the reaction, any PEP formed in the normal reaction would then be converted to pyruvate and ATP. The reaction mix contained 50 mM Tris-HCl pH 7.5, 50 μM KCl, 50 μM MgCl_2 , 25 U/mL PK, 1.5 mM ADP, 500 μM EPSP and 5 to 50 μM AroA in 50% $^2\text{H}_2\text{O}$. The reaction was allowed to equilibrate for 15 min before adding the $^2\text{H}_2\text{O}$, in order to allow the PK to scavenge any P_i in the reaction mix. Each time point was measured by diluting the reaction mix 1:100 into the MS solvent (50% MeOH in

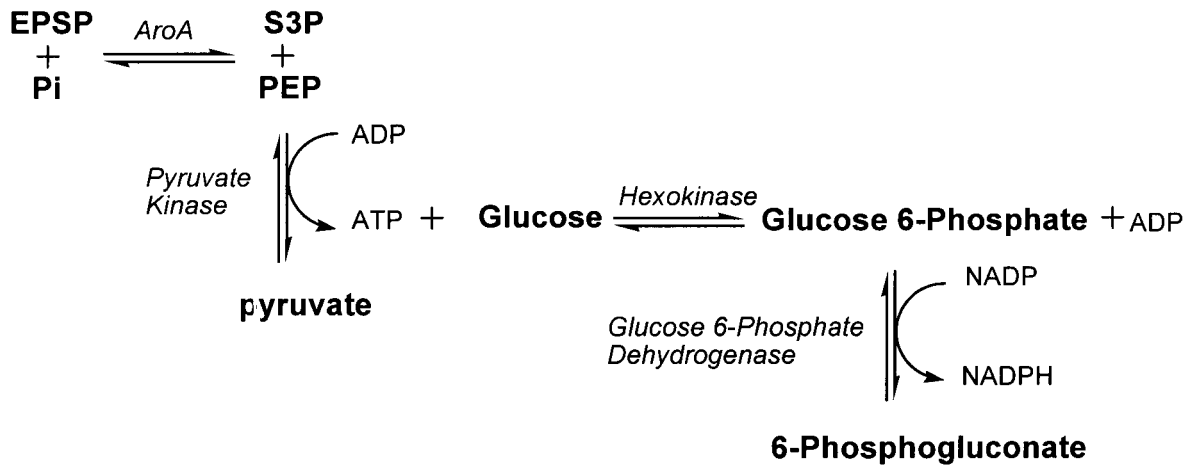
H₂O and 2.5% formic acid). The amount of ²H incorporation was calculated by the equation 1:

$$f(^2\text{H}) = (I_{324} + 2 \times I_{325}) / 2 \times (I_{323} + I_{324} + I_{325}) \quad (1)$$

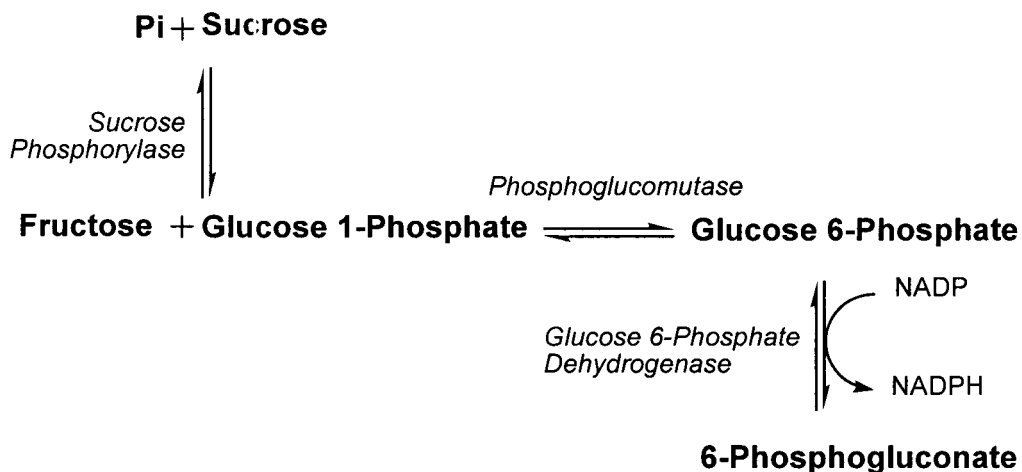
where I_{nnn} represents the area under the curve for each EPSP peak after the correction for the natural abundance of heavy isotopes.

Two other sets of coupled enzymes were used to scavenge P_i. One set coupled PK to hexokinase (HK) and glucose 6-phosphate dehydrogenase (G6PDH) (Figure 6a). The reaction mixture contained 50 mM Tris-HCl pH 7.5, 50 μM KCl, 50 μM MgCl₂, 25 U/mL PK, 1.5 mM ADP, 1 mM glucose, 0.2 mM NADP, 10 U/mL HK, 10 U/mL G6PDH, 500 μM EPSP, and 10 to 50 μM AroA in 50% ²H₂O. The last set used sucrose phosphorylase (SP), phosphoglucomutase (PGM) and G6PDH to scavenge the P_i directly (Figure 6b). This reaction mix contained 50 mM Tris-HCl, pH 7.5, 50 μM KCl, 50 μM MgCl₂, 10 U/mL SP, 1 mM sucrose, 0.2 mM NADP, 10 U/mL PGM, 10 U/mL G6PDH, 500 μM EPSP, and 10 to 75 μM AroA in 50% ²H₂O.

(a)



(b)

**Figure 6. P_i scavenging methods.**

(a) Protocol using pyruvate kinase, hexokinase, and glucose 6-phosphate dehydrogenase; (b) Protocol using sucrose phosphorylase, phosphoglucomutase, and glucose 6-phosphate dehydrogenase.

The rate of ^2H incorporation was then fitted to a first order rate equation 2:

$$A_t = A_\infty (1 - e^{-kt}) \quad (2)$$

A linear fit was used to fit the ^2H exchange with the SP, PGM and G6PDH protocol, as there was not enough ^2H incorporation to observe curvature. The k_{ex} was calculated by the equation 3:

$$k_{\text{ex}} = k_{\text{linear}} * [\text{EPSP}_o] / [\text{AroA}] \quad (3)$$

Rate of AroA-catalyzed EPSP hydrolysis

The rate of EPSP hydrolysis in the presence of AroA and all other components used in the P_i scavenging reactions was necessary in order to compare if the rate of ^2H incorporation was faster than the rate of hydrolysis. Each reaction was setup in the same manner as the P_i scavenging reactions, and 50 μL aliquots were taken at appropriate time points. Each aliquot was diluted to 100 μL with H_2O , and 100 μL of 0.4 N KOH was added to quench the reaction. The protein was removed by centrifugal ultrafiltration over 10 kDa cutoff membranes (Microcon YM10, Millipore, Corp.), for 1 hour at 12,000 x g. 150 μL was recovered from each aliquot and injected on the HPLC. The reaction components were separated using a Mono Q anion exchange column and a gradient from 100 to 700 mM ammonium bicarbonate, pH 10. The amount of EPSP remaining in each reaction was calculated from standard EPSP injections and this was used to determine the rate of hydrolysis. The rate was fitted using a single exponential decay equation 4:

$$y = A_0 e^{-kt} \quad (4)$$

The value of k_{hydro} was calculated by the equation 5:

$$k_{\text{hydro}} = k_{(\text{Eq 4})} * [\text{EPSP}_o] / [\text{AroA}] \quad (5)$$

Rate of Acid-catalyzed EPSP hydrolysis

Reactions to measure the rate of acid-catalyzed EPSP hydrolysis were set up with 500 μM EPSP and 50 mM buffer, and were run at 90 °C. The buffers used were sodium acetate (pH 4 – 6), MES (pH 4.9 – 6.9), HEPES (pH 7.2 – 8.2), CAPS (pH 8.6 – 9.7), and potassium phosphate (pH 2, 2.9, and 11.3). An unbuffered reaction at pH 14, with 1 M NaOH was also set up. The pH of these solutions was tested at 90 °C, to ensure any effect on the pH due to temperature was corrected. The results in the higher pH range were quantified by ion exchange chromatography, as these experiments were carried out over 2 to 16 days, while the lower pH range was quantified by UV spectroscopy as these reactions could be carried out in one day.

Using the HPLC, each 100 μL time point was diluted to 500 μL with 100 mM ammonium bicarbonate, pH 10, and injected on to the HPLC. The components of the reaction were separated on the Mono Q column using a gradient from 100 mM to 700 mM ammonium bicarbonate, pH 10. The amount of EPSP remaining, and S3P produced in the reaction was calculated by comparison to standard injections. This was possible as the ratios of A_{240} for S3P:PEP:EPSP had been previously determined to be 0.59:1:2.1 (Fuzhong Zhang, personal communication). The hydrolysis rate was fitted using to a single exponential decay, equation 6:

$$y=A_0e^{-kt} \tag{6}$$

Using the UV spectrophotometer, the amount of pyruvate produced in the reaction was measured by coupling the reaction to lactate dehydrogenase (LDH). A stock solution for the UV reaction was prepared with 50 mM Tris pH 7.5, 50 μ M KCl, 50 μ M MgCl₂, 10 U/mL LDH and 0.2 mM NADH. 700 μ L of this solution was added to the quartz cuvette and once a stable reading was obtained, 100 μ L time point of the reaction was added. The amount of pyruvate present at each time point was calculated by the change in A₃₄₀ in the reaction, compared to a blank with H₂O. The rate was fitted using a first order rate equation with offset, equation 7:

$$A_t = A_{\infty} (1 - e^{-kt}) + \text{offset} \quad (7)$$

Once all the rates were obtained, the pH profile of EPSP acid-catalyzed hydrolysis was also fitted in Grafit, using the double pK_a equation 8:

$$k_{hydrolysis} = \frac{k_{max} + k_{mid} 10^{(pH - pK_{a1})}}{10^{(pH - pK_{a1})} + 1} - \frac{k_{mid} 10^{(pH - pK_{a2})}}{10^{(pH - pK_{a2})} + 1} \quad (8)$$

Standard Curve on Mass Spectrometer

In order to measure KIEs by MS, it was necessary to ensure that small differences in the amount of labelled and unlabelled material in the reaction could be detected. Different calculated ratios of ¹²C EPSP:¹³C EPSP were prepared in water including, 1:1, 1:1.01, 1:1.02 and 1:1.03. These samples were injected on

the MS and the I_{323} and I_{324} were compared to determine the observed ratio. The calculated and observed ratios were plotted to ensure they fell on a straight line.

KIE by Mass Spectrometry

A method was developed to measure KIEs for acid-catalyzed EPSP hydrolysis by MS. Only the $3\text{-}^{13}\text{C}$ KIE was measured before changing to liquid scintillation counting. The reaction was 300 μL and contained 50 mM MES, pH 6.0, and 0.5 mM EPSP. The reaction was split such that 100 μL was used for the 0% reaction, and injected on the MS, while 200 μL was left at 90 $^{\circ}\text{C}$ until the reaction had reached approximately 50%. The extent of reaction was determined on the HPLC by quantifying the proportion of S3P and EPSP remaining. Before injecting on the MS, the reaction was diluted 1:100 in the MS solvent. Once the amount of ^{12}C and ^{13}C EPSP in each sample was determined, and corrected for natural abundance, the KIE was calculated using the following equation:

$$KIE = \frac{\ln\left[\frac{(1-f)(1+r_0^{-1})}{1+r_i^{-1}}\right]}{\ln\left[\frac{(1-f)(1+r_0)}{(1+r_i)}\right]} \quad (9)$$

where f is the fractional extent of reaction, r_0 is the ratio of light over heavy isotopes at 0 % of reaction, and r_i is the ratio of light over heavy isotopes at 50% of the reaction (61).

Synthesis of Radiolabelled EPSP

[¹⁴C]EPSP and [³²P]EPSP were prepared from [¹⁴C]pyruvic acid and [γ -³²P]ATP respectively. [1-¹⁴C]-, [2-¹⁴C]-, and [3-¹⁴C]-pyruvic acid are commercially available. The pyruvate reaction contained 50 mM Tris pH 7.5, 20 mM KPi, 10 mM KCl, 10 mM MgCl₂, 1.5 mM pyruvate (4-13 μ Ci), 1.5 mM ATP, 3 mM S3P, 25 μ L/mL PPDK, 15 U/ μ L PPIase, and 1 μ M AroA. The reaction was left at 37 °C overnight and typically proceeded to 50% completion. The ¹⁴C EPSP was purified on the Mono Q column using a gradient from 100 mM to 700 mM ammonium bicarbonate, pH 10, over 36 min. EPSP eluted after 37 min, and was well separated from all other peaks.

The [³²P]EPSP synthesis reaction contained 50 mM KCl, 10 mM MgCl₂, 25 mM sodium tungstate, 10 mM shikimic acid, 10 mM PEP, 2 mM [γ -³²P]ATP (50 μ Ci), 1 μ M AroA, and 100 μ L/mL AroK (shikimate kinase). This reaction was prepared, and then diluted 15-fold with H₂O in order to get the reaction to proceed, and 50 mM Hepes pH 7 was added to the final, diluted reaction. This reaction was incubated at 37 °C overnight and typically went to 50%. The ³²P EPSP was purified on the Mono Q column using a gradient from 100 mM to 700 mM ammonium bicarbonate, pH 10, over 36 min. EPSP eluted after 37 min, and was well separated from all other peaks.

KIE by Radioactivity

A method was developed to measure KIEs on the acid-catalyzed EPSP hydrolysis reaction. Each reaction was 300 μL . 100 μL was used for the 0% reaction and 200 μL was used for the 50% reaction. Each reaction contained 100,000 cpm each of the light ($[^{32}\text{P}]$ EPSP) and heavy ($[^{14}\text{C}]$ EPSP) labels. The ^{32}P label acted as a reporter on the light isotope at the position of interest, that is, ^{12}C at the same position as the ^{14}C label. The 0% and 50% reactions were purified on the HPLC using the Mono Q column and a gradient of 100 mM to 500 mM KCl in 10 mM ammonium chloride, pH 10, over 25 min, at 0.5 mL/min. Pyruvate eluted between 7 and 12 min, S3P between 12 and 15 min, and EPSP between 19 and 25 min (Figure 7). There were contaminant peaks at 10.5 min and 17.5 min, but these were never included in any of the samples used for calculation.

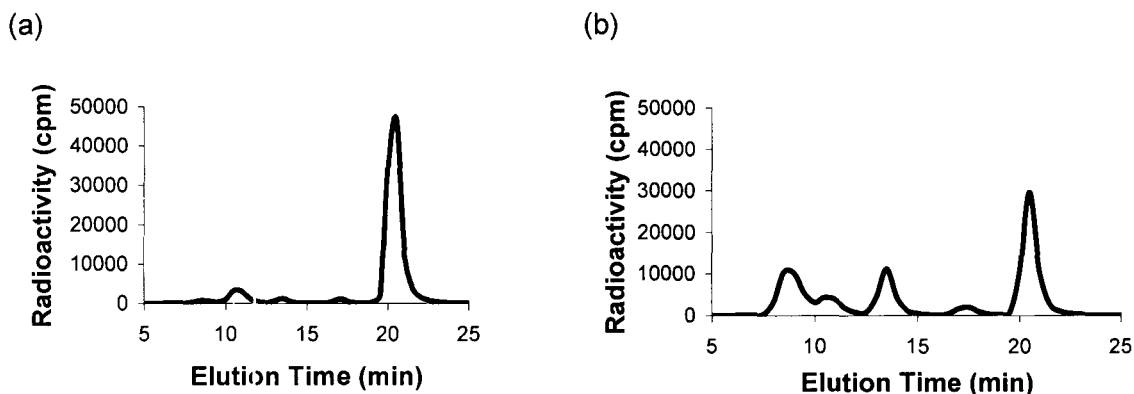


Figure 7. Radioactivity Chromatogram.

Both chromatograms show the total amount of ^{14}C and ^{32}P eluted from the HPLC. A mixture of [^{14}C] and [^{32}P] EPSP was injected on the HPLC, 0.25 mL fractions were collected, and the amount of radioactivity present in each fraction was determined by liquid scintillation counting. Equal volume of injections were done of (a) t=0 hours sample and (b) t=2 hours sample. The pyruvate peak at 9 min, and the S3P peak at 13 min increased between the 2 samples, while the EPSP peak at 20.5 min decreased.

Each peak was collected, and the sample volume was determined by weight. The volume was increased in the pyruvate and S3P samples to be equal to that of the EPSP sample with 324 mM KCl and 10 mM ammonium chloride, pH 10. The 3 samples were then split into 2 scintillation tubes each, for a total of 6 scintillation tubes, before adding 100 μL of potassium phosphate, pH 6.0, and 20 mL of Liquiscint scintillation fluid (National Diagnostic) to each tube. The volume in each tube had to be less than 1.5 mL in order to mix with the scintillation fluid without forming an emulsion. A blank sample and a standard [^{32}P]EPSP sample were also prepared with the appropriate volume of 324 mM KCl and 10 mM ammonium chloride, pH 10. All 14 tubes were counted for 10 min each to

determine the extent of reaction. This was done by comparing the amount of ^{32}P in the S3P and EPSP samples in the 0% and 50% reaction. The same calculation was made using the amount of ^{14}C in the pyruvate and EPSP samples, and this result was in good agreement with the ^{32}P extent of reaction. For measuring the KIE, only the EPSP samples from the 0% and 50% were used, as well as the blank and ^{32}P standard. These samples were counted repeatedly for 10 min each, until the 95% confidence interval of the KIE measurement was < 0.005. Equation 10 was used to calculate the KIE for each carbon position:

$$KIE = \frac{\ln \left[\frac{(1-f)(1 + \text{heavy } S_0 / \text{light } S_0)}{1 + \text{heavy } S_i / \text{light } S_i} \right]}{\ln \left[\frac{(1-f)(1 + \text{light } S_0 / \text{heavy } S_0)}{(1 + \text{light } S_i / \text{heavy } S_i)} \right]} \quad (10)$$

where f is the fractional extent of reaction, S_0 is the light or heavy isotope at the beginning of the reaction, and S_i is either the light or heavy isotope at 50% of the reaction (61).

The rate of EPSP breakdown to S3P and pyruvate was calculated from the experiments using equimolar amounts of S3P and PEP. This value was then kept fixed to determine the rate of EPSP ketal formation in the experiments using 6.7 equivalents of PEP in the presence and absence of 10 mM P_i . The results of these experiments are summarized in Table 1, and shown graphically in Figure 9. The results using KinTekSim were in good agreement with first order fits of the data (Table 1). EPSP ketal formation in these conditions demonstrates that it formed in the active site, not from dissociated THI.

Table 1. Rates of EPSP ketal formation and EPSP hydrolysis.

Values from numerical simulation using KinTekSim (62, 63). Previously determined rate constants (k_{+1} to k_{+3}) were kept fixed (28).

| Conditions | First order Fits | | Numerical Simulations | | n ^b |
|---------------------------------|--|--|--|--|----------------|
| | k_{+7} (s ⁻¹) ^a | k_{+8} (s ⁻¹) ^a | k_{+7} (s ⁻¹) ^a | k_{+8} (s ⁻¹) ^a | |
| 6.7 equiv. PEP + 10 mM P_i | $8.0 (\pm 0.4) \times 10^{-5}$ | | $5 (\pm 1) \times 10^{-5}$ | nd ^c | 3 |
| 6.7 equiv. PEP | $4.9 (\pm 0.1) \times 10^{-5}$ | | 4.3×10^{-5} | nd ^c | 1 |
| 1 equiv. PEP | $3.9 (\pm 0.9) \times 10^{-6}$ | $1.8 (\pm 0.4) \times 10^{-5}$ | $5 (\pm 2) \times 10^{-6}$ | $4 (\pm 2) \times 10^{-5}$ | 2 |
| EPSP | $1.2 (\pm 0.3) \times 10^{-5}$ | $1.4 (\pm 0.3) \times 10^{-4}$ | 1.1×10^{-5} | 1.1×10^{-4} | 1 |

^a Average from all independent trials (\pm standard deviation).

^b Number of independent trials.

^c Not determined, fixed at the average value from the trials with 1 equivalent of PEP.

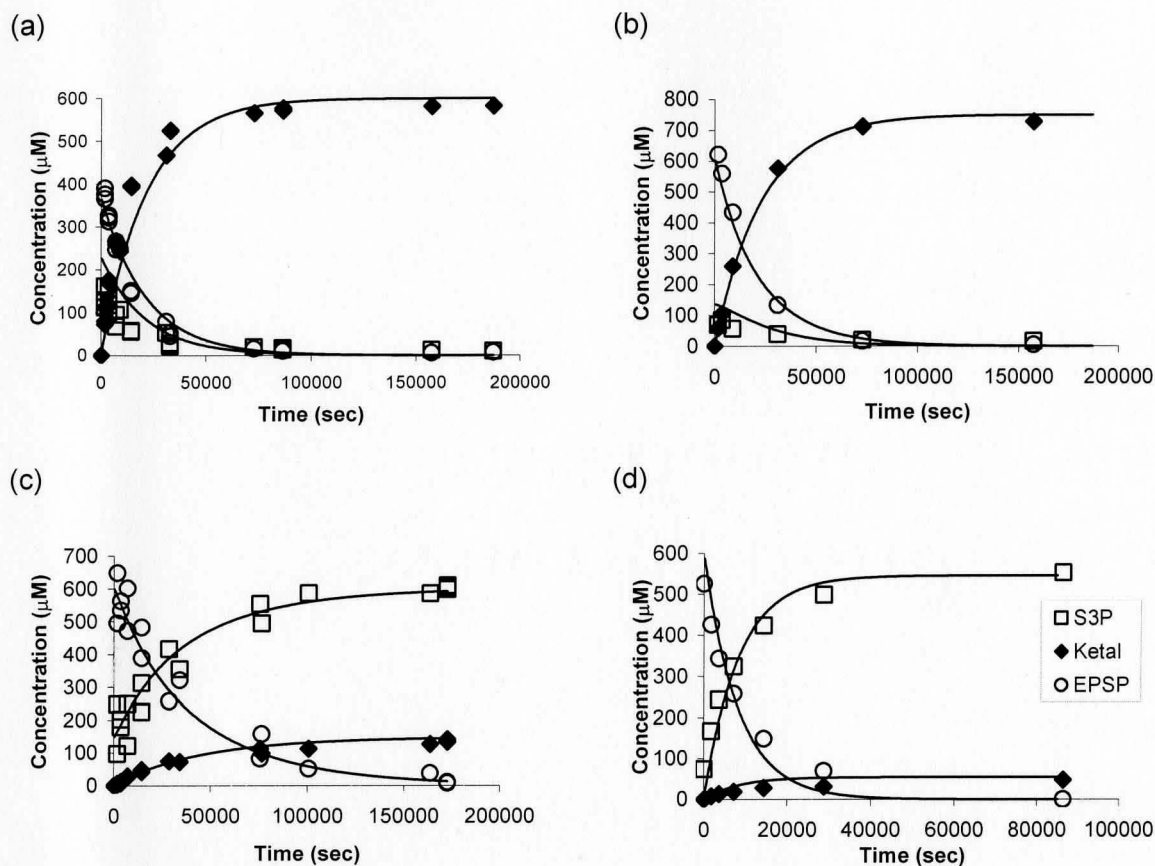


Figure 9. Reaction profiles for EPSP ketal formation under different conditions.

(a) excess PEP + 10 mM P_i (S3P:PEP:AroA = 1:6.7:1.33). (b) excess PEP (S3P:PEP:AroA = 1:6.7:1.33). (c) equimolar PEP and S3P (1:1:1.33). (d) no PEP (EPSP:AroA = 1:1.33). Solid lines were calculated from numerical simulations using the rate constants in Table 1 and (28).

Confirmation of EPSP Ketal Structure

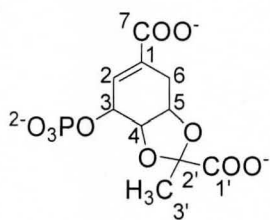
Unlabelled EPSP ketal was synthesized under the same conditions as the excess AroA experiments, in order to confirm the structure by NMR. The NMR results are summarized in Table 2 and Figure 10-13.

Table 2. Chemical shifts and coupling constants for EPSP ketal, shikimate 3-phosphate, and shikimic acid.

| Compound | Atom no. ^a | δC (ppm) | δH (ppm) | J (H, H) | J (Hz) |
|------------------------------|-----------------------|------------------------|------------------------|---------------|--------|
| EPSP ketal | | | | | |
| | 1 | 137.5 | | | |
| | 2 | 128.9 | 6.46 | J (H2, H6b) | 2.6 |
| | | | | J (H2, H3) | 5.2 |
| | 3 | 65.9 | 4.96 | J (H3, H2/H4) | 4.2 |
| | | | | J (H3, P) | 7.5 |
| | 4 | 78.8 | 3.56 | J (H4, H5) | 10.3 |
| | | | | J (H4, H3) | 3.4 |
| | 5 | 71.1 | 4.00 | J (H5, H6b) | 10.3 |
| | | | | J (H5, H6a) | 5.3 |
| | | | | J (H5, H4) | 10.3 |
| | 6a | 30.9 | 2.90 | J (H6a, H5) | 5.3 |
| | | | | J (H6a, H6b) | 16.5 |
| | 6b | | 2.29 | J (H6b, H2) | 2.6 |
| | | | | J (H6b, H5) | 10.4 |
| | | | | J (H6b, H6a) | 16.5 |
| | 7 | 174.6 | | | |
| | 1' | 176.9 | | | |
| | 2' | 107.8 | | | |
| | 3' | 22.3 | 1.54 | | |
| Shikimate 3-phosphate | | | | | |
| | 1 | 135.4 | | | |
| | 2 | 129.3 | 6.46 | J (H2, H6) | 1.9 |
| | | | | J (H2, H3) | 4.0 |
| | 3 | 66.6 | 4.83 | J (H3, H2/H4) | 4.2 |
| | | | | J (H3, P) | 8.5 |
| | 4 | 70.2 | 3.85 | J (H4, H3) | 4.1 |
| | | | | J (H4, H5) | 8.0 |
| | 5 | 70 | 4.07 | J (H5, H6ab) | 5.8 |
| | | | | J (H5, H4) | 8.0 |
| | 6a | 31.1 | 2.70 | J (H6a, H2) | 1.7 |
| | | | | J (H6a, H5) | 5.3 |
| | | | | J (H6a, H6b) | 18.2 |
| | 6b | | 2.21 | J (H6b, H2) | 1.9 |
| | | | | J (H6b, H5) | 6.3 |
| | | | | J (H6b, H6a) | 18.2 |
| | 7 | 174.5 | | | |
| Shikimic acid | | | | | |
| | 1 | 129.1 | | | |
| | 2 | 136.7 | 6.82 | J (H2, H6) | 1.8 |

| | | | | |
|----|-------|------|----------------|------|
| 3 | 65.2 | 4.44 | J (H2, H3) | 4.0 |
| | | | | 1.6 |
| | | | | 1.7 |
| | | | | 2.4 |
| 4 | 70.5 | 3.76 | J (H4, H5) | 8.2 |
| | | | J (H4, H3) | 4.3 |
| 5 | 66.0 | 4.29 | J (H5, H6a) | 5.3 |
| | | | J (H5, H6b) | 6.4 |
| | | | J (H5, H4) | 8.3 |
| | | | J (H6a, H2/H3) | 1.7 |
| 6a | 29.8 | 2.72 | J (H6a, H5) | 5.3 |
| | | | J (H6a, H6b) | 18.1 |
| | | | J (H6b, H2/H3) | 2.0 |
| 6b | | 2.21 | J (H6b, H5) | 6.5 |
| | | | J (H6b, H6a) | 18.1 |
| | | | | |
| 7 | 169.0 | | | |

a



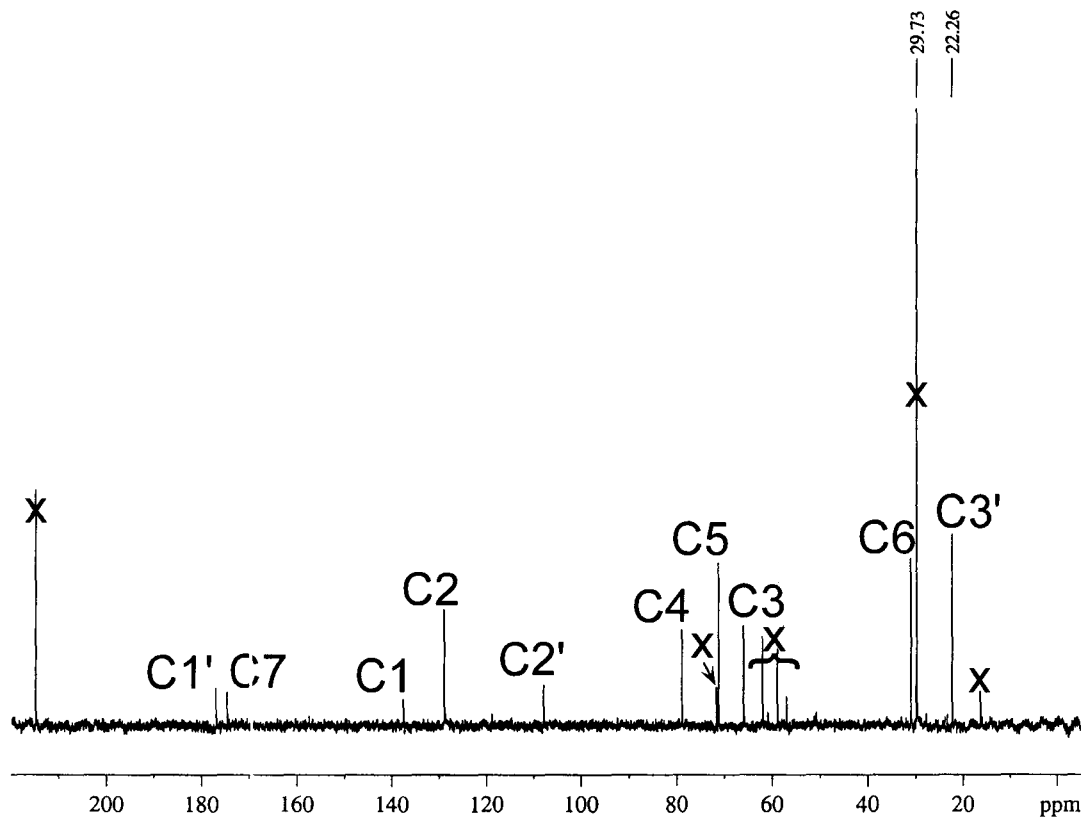


Figure 11. ^{13}C spectrum of EPSP ketal.

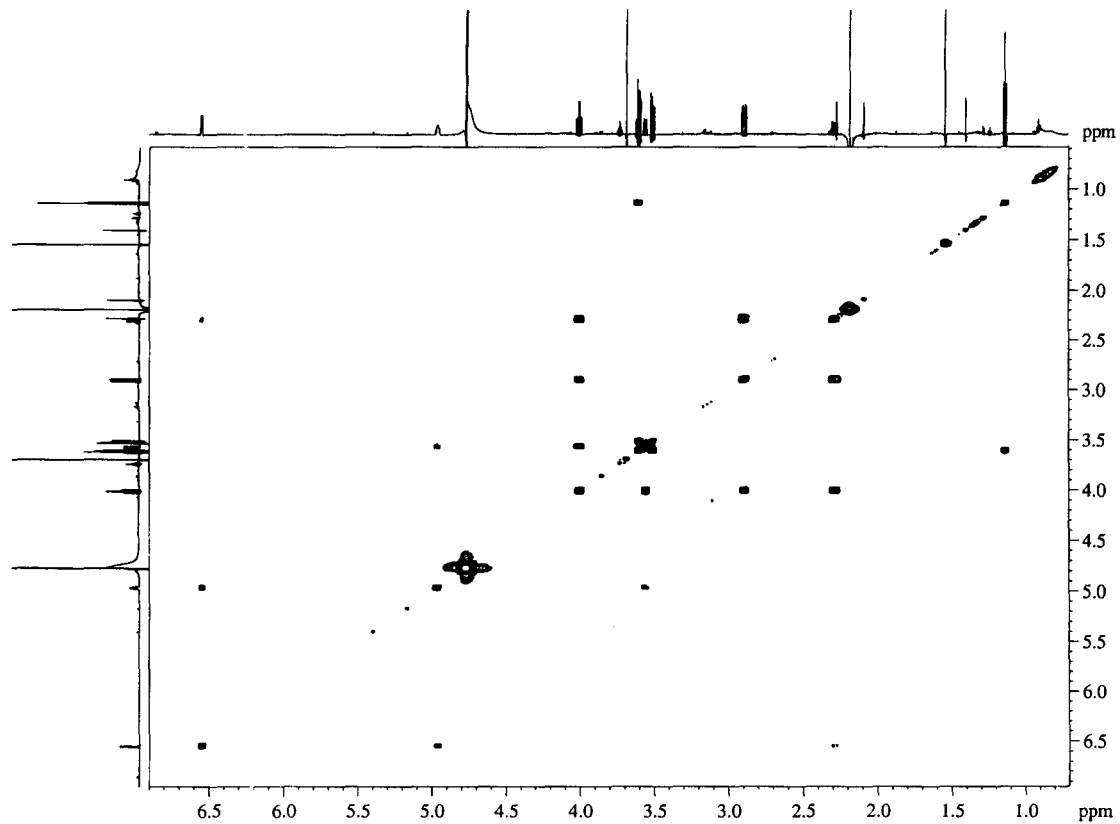


Figure 12. Gradient Proton COSY 2-D NMR spectrum of EPSP ketal.

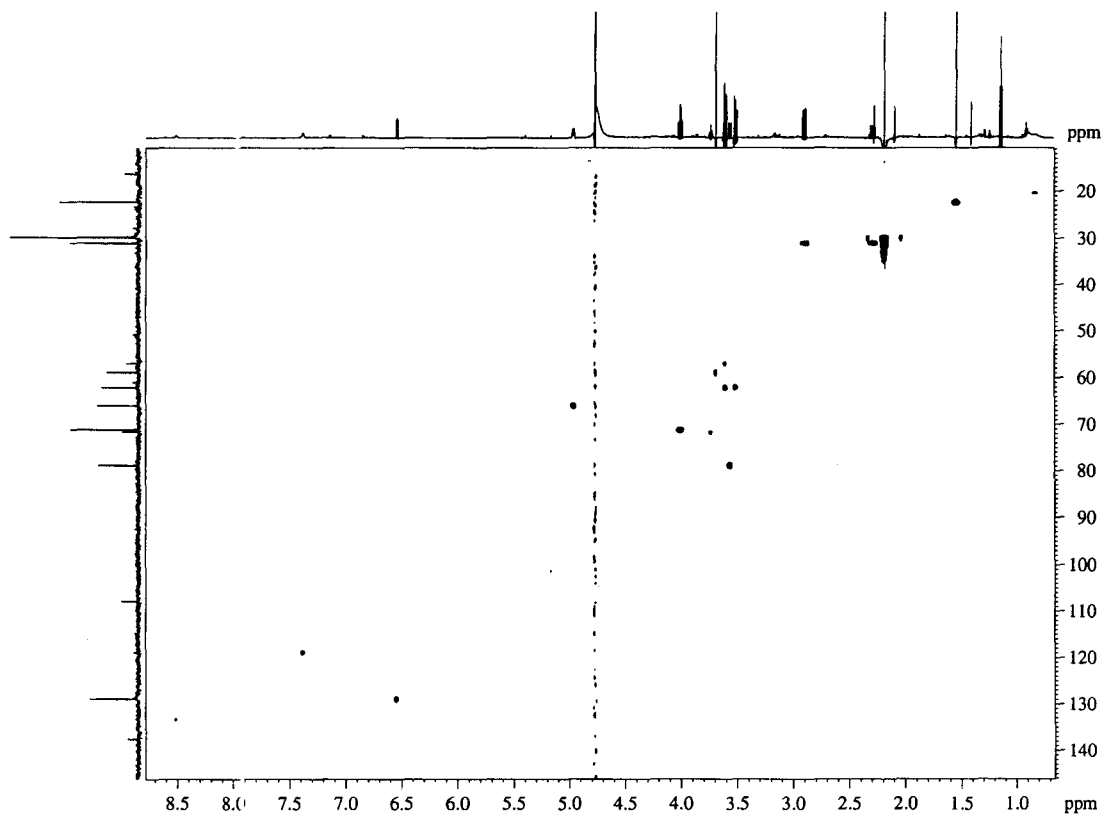


Figure 13. ^1H - ^{13}C Gradient HSQC spectrum of EPSP ketal.

Acid-catalyzed EPSP hydrolysis

The pH-dependence of acid-catalyzed EPSP hydrolysis was determined in the range of pH 2-14 at 90 °C (Figure 14). The rate of hydrolysis at pH 14 was not detectable, even after 16 days. A trend can be seen where the rate of hydrolysis increases with lower pH. This data fit well to an equation which depends on two ionizing groups. The first observed pK_a of 4.0 ± 0.3 was assigned to the ionization of the C1' carboxylate group, while the second observed pK_a of 6.5 ± 0.3 most likely reflects the ionization state of the 3-phosphate group. The first observed pK_a is in good agreement with a previous study of acid-catalyzed vinyl ether hydrolysis, including EPSP, which was 3.77 at 25 °C at an ionic strength of 0.1 M (64).

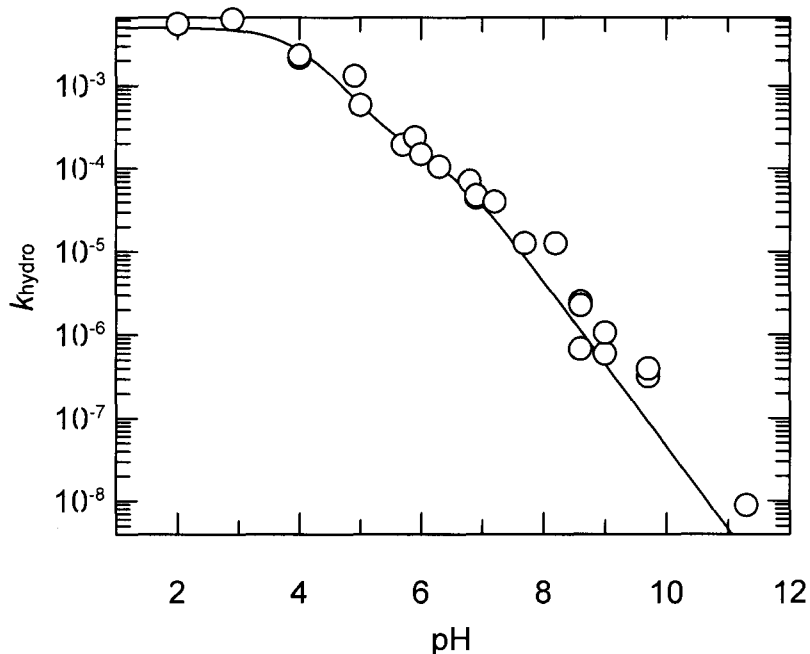


Figure 14. pH profile of Acid-Catalyzed EPSP Hydrolysis.

The rate of EPSP hydrolysis at 90 °C was determined in various buffer conditions from pH 2 to pH 11.3. The pH of each buffer was corrected for the elevated temperature of the reaction.

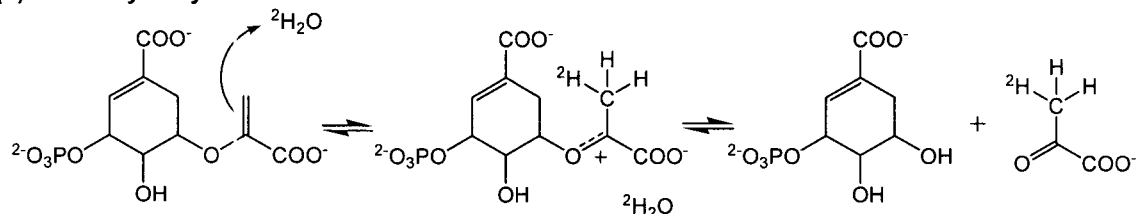
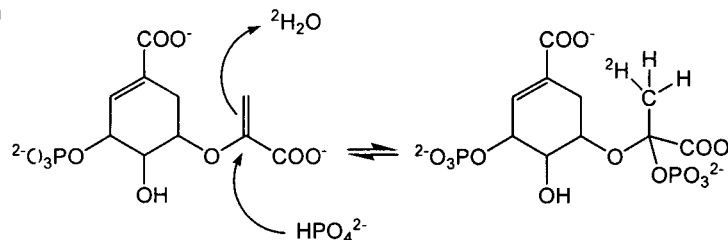
Rate of ^2H incorporation

EPSP ketal formation provides some evidence for the formation of a cationic intermediate as part of the normal AroA mechanism, though it is also consistent with cation-like, but formally concerted, addition step. In order to further probe the reaction, the rate of ^2H incorporation from $^2\text{H}_2\text{O}$ into EPSP during EPSP hydrolysis was studied. If there is ^2H incorporation into EPSP in the presence of AroA, this would be independent evidence for reversible cationic intermediate formation. If there is no incorporation, this would be consistent with irreversible cationic intermediate formation (i.e., a cationic intermediate is formed, but it always proceeds forward to products), as well as a concerted mechanism

with irreversible water attack concomitant with protonation. If there is no incorporation, then we have a new method for measuring KIEs on the EPSP hydrolysis mechanism, as EPSP hydrolysis is irreversible.

P_i Scavenging

The challenge with the ²H incorporation experiments was to ensure there was no P_i present in the reaction mixture. If any P_i were present, it would be incorporated into the normal AroA reaction and form THI reversibly (Figure 15b). THI would breakdown to EPSP, with ²H incorporation resulting. It was essential that no THI was formed, so that any observed ²H incorporation into EPSP would be strictly from an equilibrium between EPSP and the cationic intermediate (Figure 15a).

(a) EPSP Hydrolysis:**(b) THI formation****Figure 15. Mechanism of ^2H incorporation.**

(a) In the presence of AroA, EPSP will be hydrolyzed, and if there is any ^2H detected in EPSP, then we know an equilibrium exists between EPSP and a cationic intermediate.

(b) If there is any P_i present under these conditions, THI will form from EPSP and P_i , but a stepwise or concerted reaction will not be discernable.

It is possible to carry out these experiments on the MS, as each ^2H incorporated into EPSP would lead to an increase of one in the m/z value. Before the addition of $^2\text{H}_2\text{O}$ to each experiment, an injection was done to determine the natural abundance in the unlabelled substrate (Figure 16a). Subsequent injections were done at set time points in order to measure the shift in peak intensities, which corresponded to the incorporation of ^2H into EPSP (Figure 16b).

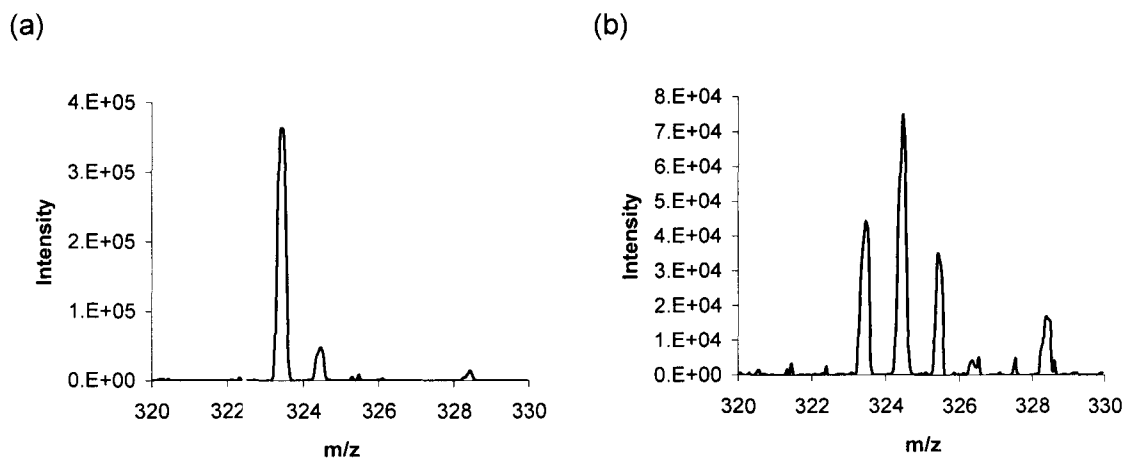


Figure 16. Measurement of ^2H incorporation.

(a) Natural abundance ratio of EPSP before addition of $^2\text{H}_2\text{O}$, (b) Representative spectrum of ^2H incorporation into EPSP, 120 min after $^2\text{H}_2\text{O}$.

Because low levels of P_i are ubiquitous, scavenging systems were set up to remove any P_i from the AroA and EPSP reaction mixtures. Three sets of coupled enzymes were used in order to scavenge P_i . It was necessary to equilibrate the EPSP hydrolysis reaction with these enzymes in H_2O for 15 min to allow all the P_i to be scavenged from the system before adding $^2\text{H}_2\text{O}$.

The first P_i scavenging system used pyruvate kinase (PK) and ADP, to convert any PEP to pyruvate and ATP. When using this system to scavenge P_i , all three components, ADP, PK and AroA, were varied. There was not a large difference in the exchange rate between 0.3 and 3 mM ADP, and therefore 1.5 mM was used (Figure 17a). PK concentration was varied between 5 and 125 U/mL. At low PK concentrations, <10 U/mL, scavenging was not complete before the $^2\text{H}_2\text{O}$ was added. At 125 U/mL, exchange was also fast, possibly because

PK was hydrolyzing ATP, to produce P_i . Exchange was minimal between 25 and 50 U/mL (Figure 17b). Under these conditions, AroA-catalyzed 2H exchange occurred, which was inhibited upon addition of glyphosate. In order to test whether this exchange was due to the continued presence of P_i , another scavenging system was used.

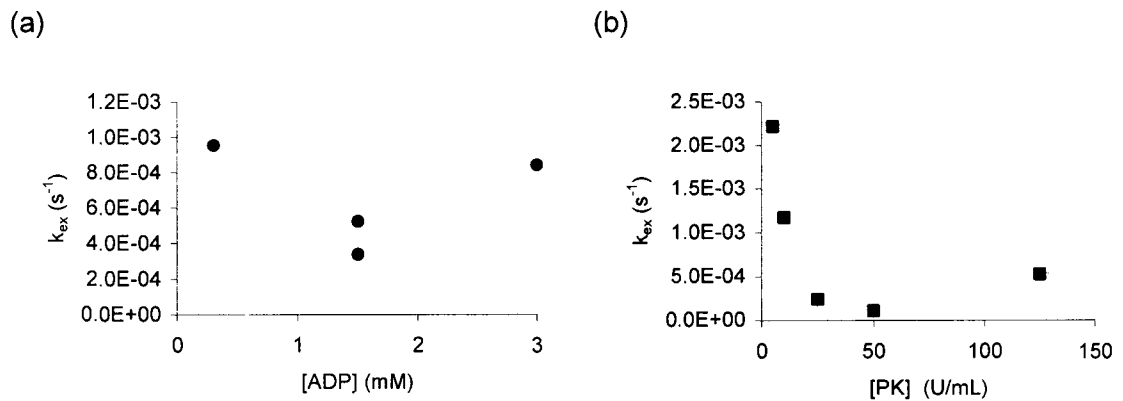


Figure 17. Controls for 2H incorporation.

Determined the appropriate amounts of (a) ADP and (b) PK to add to the reaction mix.

HK and G6PDH were added to the PK scavenging system. With this PK, HK and G6PDH system, the 2H exchange rate was reduced relative to PK alone, and was still dependent on the concentration of AroA (Figure 18a and 18b).

However, with the SP, PGM and G6PDH scavenging system, exchange was essentially stopped (Figure 18c). Even with increasing concentrations of AroA, there was no difference in the rate of 2H incorporation. AroA was not inhibited with these conditions, as EPSP hydrolysis was still catalyzed. Thus, these experiments showed that AroA hydrolyzes EPSP without catalyzing 2H exchange.

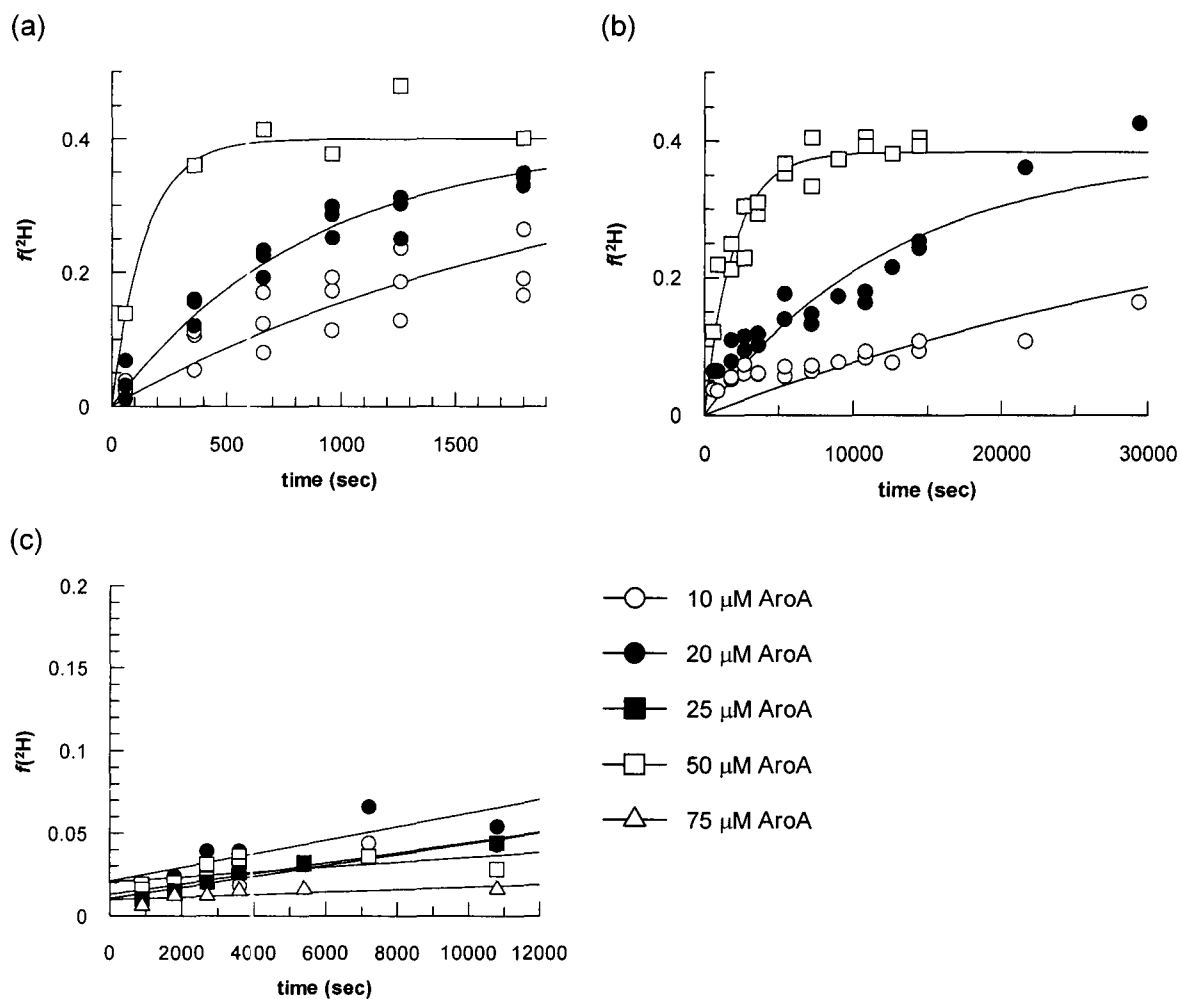


Figure 18. P_i Scavenging experiments.

Three different methods to scavenge P_i were used in order to ensure all P_i was removed from the solution; (a) PK alone, (b) PK, HK, and G6PDH and (c) SP, PGM and G6PDH. Different concentrations of AroA were used.

The rate of EPSP hydrolysis was determined under the same conditions as the ^2H exchange reaction in order to calculate the exchange:hydrolysis ratio, $k_{\text{ex}}/k_{\text{hyd}}$ (Table 3).

Table 3. AroA-Catalyzed ^2H incorporation versus EPSP Hydrolysis.

The rate of EPSP hydrolysis (k_{hyd}) was determined under the same conditions as the rate of ^2H exchange on the MS (k_{ex}). Three conditions were tested in order to ensure that all P_i was scavenged: (a) PK only, (b) PK, HK and G6PDH, and (c) SP, PGM and G6PDH.

| | (a) | (b) | (c) |
|--------------------------------|--------------------------------|--------------------------------|--------------------------------|
| $k_{\text{hyd}}^{\text{a}}$ | $3.0 (\pm 0.6) \times 10^{-4}$ | $2.3 (\pm 0.1) \times 10^{-4}$ | $6.7 (\pm 1.0) \times 10^{-4}$ |
| k_{ex}^{b} | $4.1 (\pm 2.5) \times 10^{-2}$ | $2.7 (\pm 2.1) \times 10^{-3}$ | $6.9 (\pm 6.3) \times 10^{-5}$ |
| $k_{\text{ex}}/k_{\text{hyd}}$ | 130 | 12 | 0.1 |

^a. Rate of hydrolysis \pm Standard Deviation

^b. Average Rate of ^2H exchange \pm Standard Deviation

Standard Curve on Mass Spectrometer

The results of the ^2H incorporation and P_i scavenging experiments indicated that protonation was the first irreversible step of EPSP hydrolysis. This provided reaction conditions under which to measure KIEs on the enzyme-catalyzed EPSP hydrolysis reaction. In order to measure KIEs by MS, it was necessary to be able to reliably detect very small changes in the ratio of unlabelled and labelled species. This was tested by mixing ^{12}C and ^{13}C EPSP in a known ratio and injecting this mixture on the MS. The calculated ratio was compared to the observed ratio in Figure 19. With the slope of this curve being essentially 1, this met the criteria to confidently measure small changes in the $^{12}\text{C}:^{13}\text{C}$ ratio.

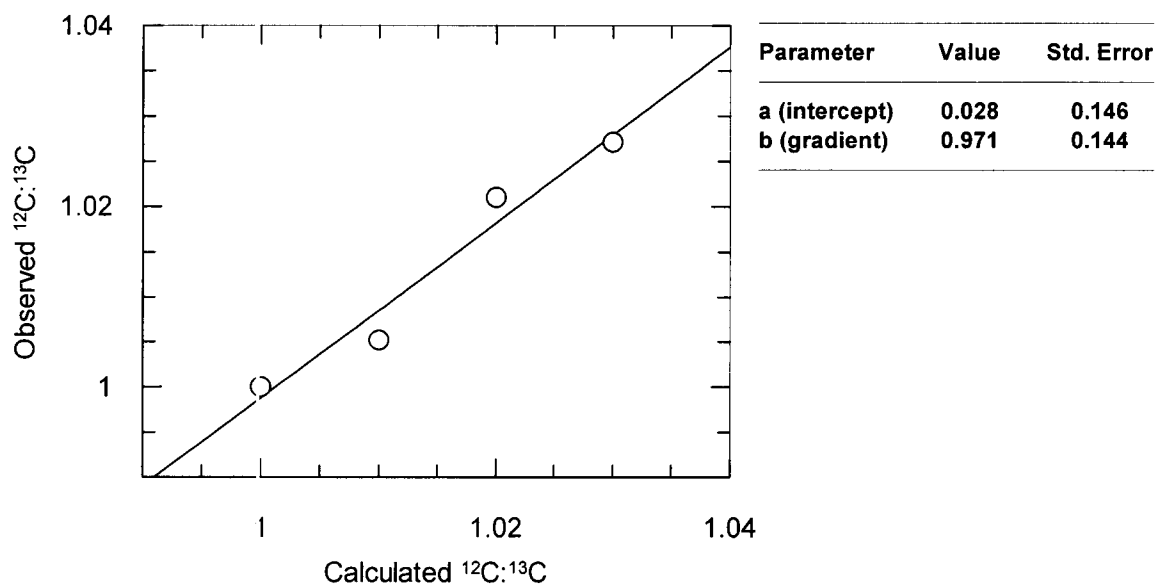


Figure 19. Standard curve on mass spectrometer.

A known ratio of $^{12}\text{C}:^{13}\text{C}$ EPSP was calculated and inject on the MS. This was compared to the observed peak intensities in the MS spectrum.

KIE by Mass Spectrometry

A MS method was developed to measure KIEs on acid-catalyzed EPSP hydrolysis. Using labelled ^{13}C -EPSP, this method was tested in four separate trials (Table 4). Given the large variation between the experiments using MES as buffer, and the large difference in the result with NaOAc as buffer, this method was abandoned in favour of using radiolabelled EPSP and determining KIE by liquid scintillation counting.

Table 4. [3-¹³C] EPSP KIEs for acid catalyzed EPSP hydrolysis measured by mass spectrometry.

| Sample # (buffer used) | Extent of Reaction (<i>f</i>) | ¹² C/ ¹³ C | ¹² C/ ¹³ C | KIE |
|---------------------------|------------------------------------|--|--|-------|
| | | Ratio for Unreacted EPSP (<i>r</i> _o) | Ratio for Reacted EPSP (<i>r</i> _i) | |
| 1 (MES) | 0.238 | 0.868 | 0.860 | 1.034 |
| 2 (MES) | 0.415 | 0.868 | 0.848 | 1.044 |
| 3 (MES) | 0.486 | 0.857 | 0.844 | 1.023 |
| 4 (NaOAc) | 0.363 | 0.907 | 0.969 | 0.862 |

KIE by Liquid Scintillation Counting

The method to measure KIEs on acid-catalyzed EPSP hydrolysis reaction by radioactivity was tested at 3 carbon positions. The measurements were done in two different buffers, MES and NaOAc. When using MES more than six months old, the KIE results were very different (Data not shown). When freshly prepared MES was used (Sample 1), similar results to NaOAc were obtained (Sample 2 and 3). The results are summarized in Table 5-7.

Table 5. [1-¹⁴C] EPSP KIEs for acid-catalyzed EPSP hydrolysis.

Three independent trials were conducted and the average of these 3 trials \pm 95% confidence interval is reported.

| Sample # | Extent of Reaction (f) | KIE |
|----------|------------------------|-------------------|
| 1 | 0.441 | 0.966 |
| 2 | 0.515 | 0.960 |
| 3 | 0.500 | 0.965 |
| | Average | 0.964 \pm 0.004 |

Table 6. [2-¹⁴C] EPSP KIEs for acid-catalyzed EPSP hydrolysis.

Three independent trials were conducted and the average of these 3 trials \pm 95% confidence interval is reported.

| Sample # | Extent of Reaction (f) | KIE |
|----------|------------------------|-------------------|
| 1 | 0.473 | 0.971 |
| 2 | 0.510 | 0.963 |
| 3 | 0.505 | 0.964 |
| | Average | 0.966 \pm 0.005 |

Table 7. [3-¹⁴C] EPSP KIEs for acid-catalyzed EPSP hydrolysis.

Three independent trials were conducted and the average of these 3 trials \pm 95% confidence interval is reported.

| Sample # | Extent of Reaction (f) | KIE |
|----------|------------------------|-------------------|
| 1 | 0.457 | 0.973 |
| 2 | 0.620 | 0.978 |
| 3 | 0.434 | 0.985 |
| | Average | 0.979 \pm 0.007 |

Discussion

EPSP Ketal formation

Previous studies of the AroA mechanism proposed that EPSP ketal formed from dissociated THI breaking down in solution (28, 32). Our lab's study of the non-enzymatic THI breakdown, demonstrated that too little EPSP ketal formed to account for the amounts observed previously in enzymatic reactions (27). The experiments described here were designed to eliminate any non-enzymatic source of EPSP ketal, and thus to demonstrate whether it was formed in the AroA active site. In each of the reaction conditions containing excess AroA, EPSP ketal formed; with excess PEP, the EPSP ketal yield was > 95%. This effectively eliminated non-enzymatic THI breakdown, and showed that EPSP ketal was formed in the AroA active site. This begins to support the hypothesis that a cationic intermediate exists as part of the normal enzymatic mechanism of AroA.

The ratio of k_{cat}/k_7 (where $k_{\text{cat}} = 57 \text{ s}^{-1}$ (12)) shows that EPSP ketal forms once every 10^6 enzymatic turnovers, therefore one could argue that formation of EPSP ketal is a rare catalytic mistake. However, the fact that EPSP ketal formed 8% of the products in the EPSP hydrolysis reaction shows that it is not a rare catalytic mistake. This suggests that the cationic intermediate forms at least 8% of the time. It most likely forms 100% of the time, and it is merely the availability of the nucleophile which dictates the product distribution.

Nucleophile vs. Electrophile Activation

EPSP ketal formation on the enzyme does not distinguish if the reaction is catalyzed by nucleophile activation or *enol*/pyruvyl activation. There is no good evidence for or against nucleophile activation in AroA, though a priori it is a reasonable mechanistic proposal. The results of this study of non-enzymatic EPSP breakdown at pH 14 shows that it is not susceptible to nucleophile catalysis without prior or simultaneous *enol*/pyruvyl activation. Even if AroA does employ nucleophile activation for P_i addition to EPSP or even H_2O in EPSP hydrolysis, this same mechanism could not be used to activate the O4H nucleophile. From the crystal structures, we know the O4H is on the opposite side of the molecule relative to phosphate. Therefore, in order to have the intramolecular reaction occur, the *enol*/pyruvyl group must first be activated, leading to the formation of an unstable cationic intermediate. The formation of this intermediate would still allow for the other nucleophiles to attack, and the only way that EPSP ketal could be forming under these conditions is through *enol*/pyruvyl activation (Figure 20).

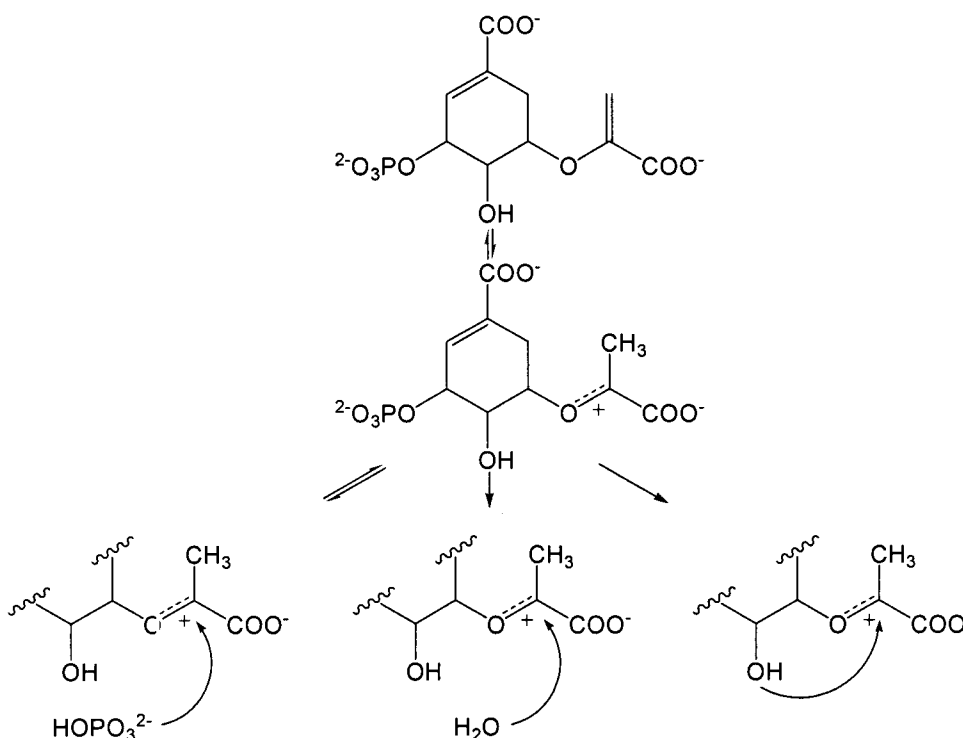


Figure 20. Fate of the EPSP Cation.

Following the protonation of C3', several nucleophiles can attack.

There is also evidence in the literature for the formation of a cationic intermediate in both the addition and elimination step of the AroA reaction. It has been observed that the C3 protons of PEP will exchange with the solvent in the presence of 4,5-cideoxy-S3P (20). Since this substrate analogue lacks the nucleophilic O4H group, AroA must undergo a conformation change which could allow for the formation of a cationic intermediate in the addition step.

Catalytic Advantage of Acid Catalysis

In previous work on vinyl ether hydrolysis (64), the rate enhancement of EPSP hydrolysis due to acidic conditions was studied. These results showed a change in pH from pH 4.8 up to 60% HClO₄, lead to a rate enhancement of 10⁶.

There was no plateau in the rate at 60% HClO₄, therefore the actual rate enhancement is >10⁶ and this predicted rate enhancement is actually quite conservative.

In the current study, the pH profile was extended to basic pH's, up to a value of pH 14 (Figure 14). The same plateau seen by Kresge between pH 0 and 3, was seen in the first measurement done between pH 2 and 4. This plateau can be attributed to the change of the carboxylic acid becoming a carboxylate functional group. The change from an electron withdrawing to an electron donating group, will cause an increased stabilization of the cation.

Over the pH range of this study, from pH 2 to 11.3, there was a rate enhancement of EPSP hydrolysis on the order of 10⁵. At pH 14, there was no detectable measured rate, even after reacting for 16 days. It would have been possible to reliably measure a 5% change in the reaction, and therefore the reaction rate at pH 14 was < 4 × 10⁻⁸ s⁻¹. By combining the results in these two studies, it is possible to predict a rate enhancement of at least 10⁸ over the full pH range. Without having the upper or lower limits of the profile well defined, the rate enhancement is actually >10⁸.

The rate enhancement of EPSP hydrolysis due to pH shows that acid catalysis has a dramatic effect on this reaction. By first protonating EPSP, and activating the *enol*/pyruvyl group, this would decrease the amount of energy required by AroA to catalyze the reaction.

Energetic cost of EPSP cation formation

There is a considerable energetic cost in the formation and stabilization of this cationic intermediate. Assuming $pK_a < -4$ (64), then protonation of this carbon at physiological pH corresponds to > 15 kcal/mol of energy exerted by the enzyme to form this intermediate. If we can capture a fraction of the binding energy the enzyme uses to stabilize the putative EPSP cation, this is a good starting point for inhibitor design. This would provide another piece of the puzzle in understanding how to better inhibit AroA.

^2H Incorporation

In order to provide an independent line of evidence to support the formation of a cationic intermediate, AroA-catalyzed EPSP hydrolysis in the presence of $^2\text{H}_2\text{O}$ was investigated. ^2H incorporation into EPSP in the presence of AroA would support the hypothesis of reversible cationic intermediate formation. It is essential there be no P_i present under these conditions, as this would allow THI formation and therefore ^2H exchange. If any ^2H is incorporated into EPSP, this would provide evidence for an equilibrium between EPSP and a cationic intermediate.

Under two of the three P_i scavenging systems tested, the ^2H exchange rate was faster than AroA-catalyzed EPSP hydrolysis. However, under the reaction conditions with SP, PGM, and G6PDH there was negligible ^2H exchange in comparison to AroA-catalyzed hydrolysis. The PK and the PK, HK and

G6PDH systems were not as efficient at scavenging P_i . Both these methods indirectly scavenged P_i , as they depended on AroA to convert any P_i in solution first to PEP. Using SP, PGM and G6PDH, P_i was scavenged directly from solution. Considering these results taken together, the PK-based scavenging systems did not work. There was THI formation under these reaction conditions, and therefore 2H exchange was not due to an equilibrium with an EPSP cation.

The mechanistically relevant information from these experiments was that they defined the first irreversible step of this reaction and therefore provided a method to measure KIEs on this reaction. In the presence of SP, PGM and G6PDH, there is negligible 2H incorporation into EPSP. Therefore, upon protonation of EPSP, the reaction is essentially irreversible. Since the first irreversible step of the reaction is known, it is possible to measure KIEs on this step in the reaction.

These experiments defined the reaction conditions to measure KIEs on the enzyme-catalyzed reaction. It is important to also measure KIEs on the non-enzymatic reaction in order to know specifically what the enzyme is doing to lower the activation energy of the TS. The non-enzymatic reaction was studied first, in order to develop the best method to make all the KIE measurements.

KIE interpretations

From the 2H incorporation experiments on the enzyme-catalyzed reaction, with an efficient P_i scavenging method, there was a negligible amount of

exchange compared to hydrolysis. This suggested that protonation was the first irreversible step in AroA-catalyzed EPSP hydrolysis, followed by nucleophile attack. This type of reaction can again be drawn using a More O'Farrell – Jencks reaction diagram (Figure 21). Here, the subscript H represents the proton, and again, it is not yet possible to predict the precise mechanism of the reaction. Once KIEs are measured for this reaction, it will be possible to determine if this reaction follows a stepwise mechanism, with the formation of a discrete cationic intermediate (Figure 22a), or if it follows a more concerted mechanism, with protonation and water attack occurring simultaneously (Figure 22b).

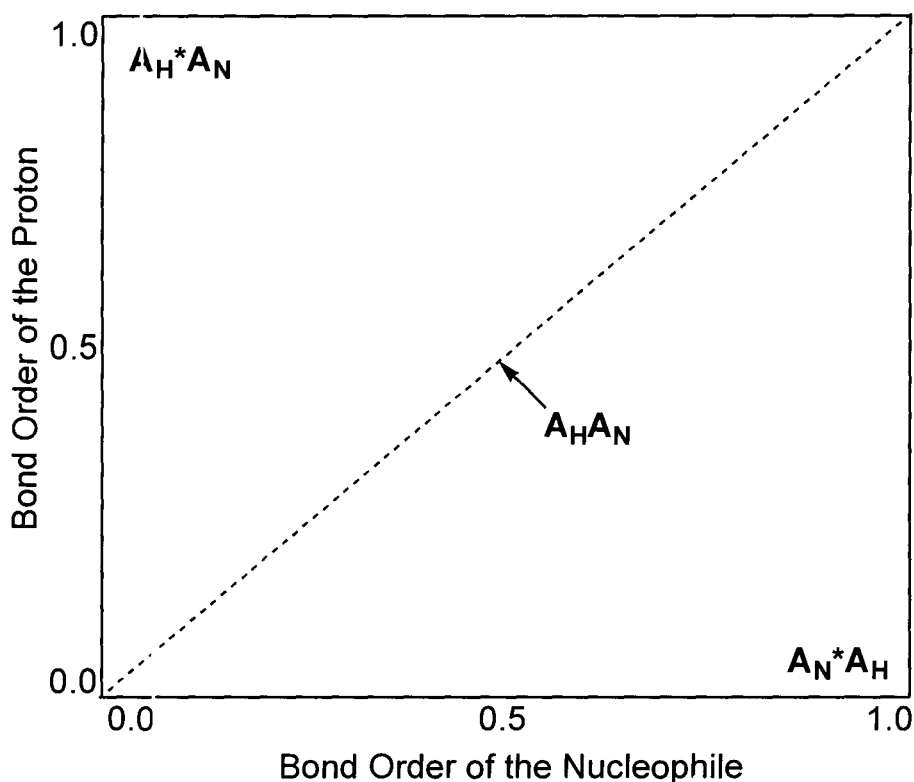
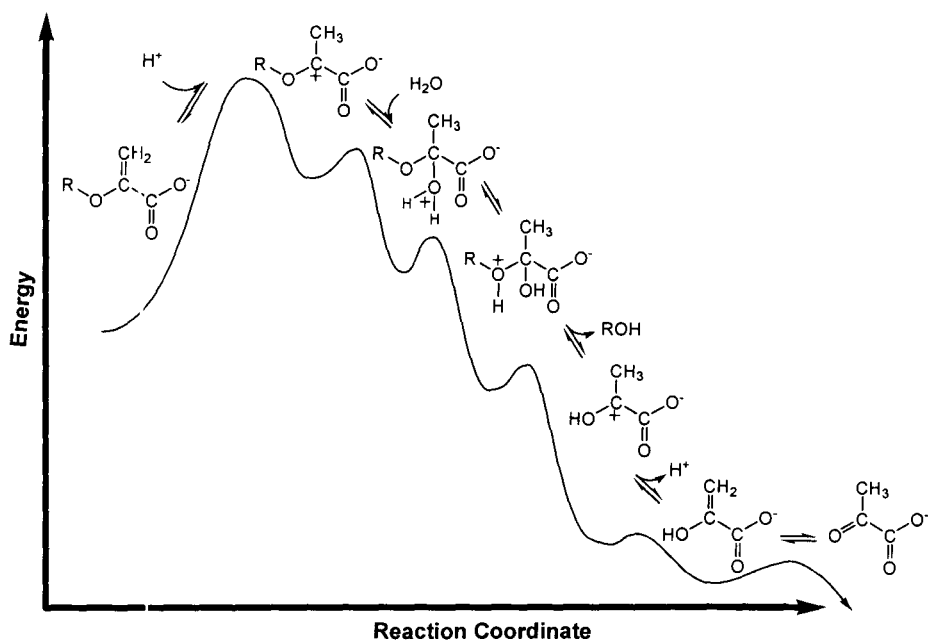


Figure 21. Reaction Space diagram of the initial steps of the AroA-catalyzed reaction.

(a)



(b)

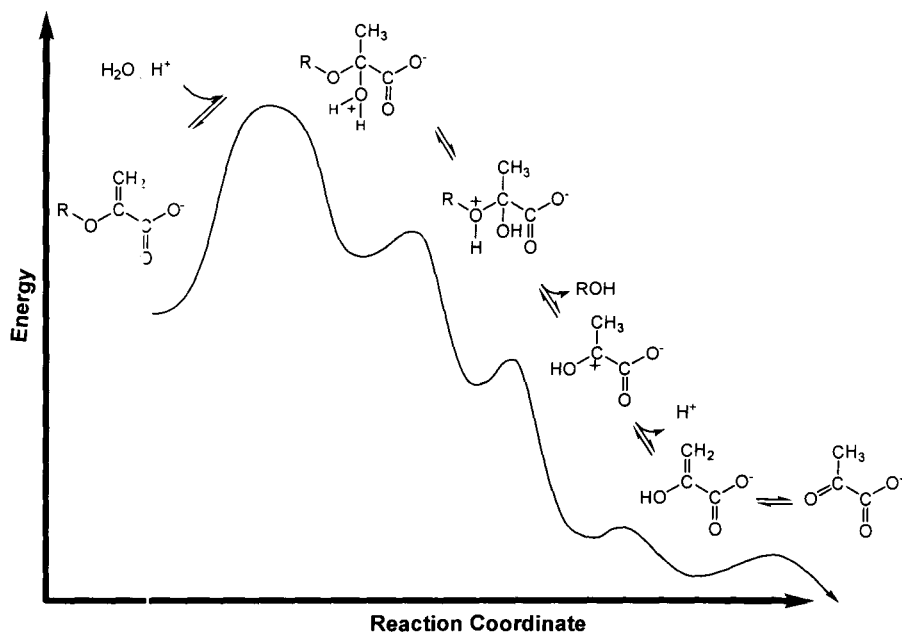


Figure 22. Reaction coordinate of AroA-catalyzed EPSP hydrolysis.

(a) Stepwise mechanism, ($A_H^*A_N$ in the first step); (b) Concerted mechanism, ($A_H A_N$ in the first step)

KIE measurements of the acid-catalyzed reaction have been completed on the three carbon positions on EPSP by liquid scintillation counting. Each of these positions was measured 3 times, in 2 different buffers, and demonstrated good reproducibility. This method was chosen in favour of whole molecule MS KIEs, which did not show good reproducibility, and demonstrated a buffer dependence on the results.

Each carbon position measured showed an inverse KIE (Figure 23). This means that each carbon is going from a looser vibrational environment in the EPSP substrate to a tighter vibrational environment at the TS. It is unusual that all three carbons would be going into a more constrained environment. This is supported however, from previous studies in our group of both AroA and MurA, where similar results were obtained using MS, with the three *enolpyruvyl* carbons having inverse KIEs (Fuzhong Zhang, personal communication).

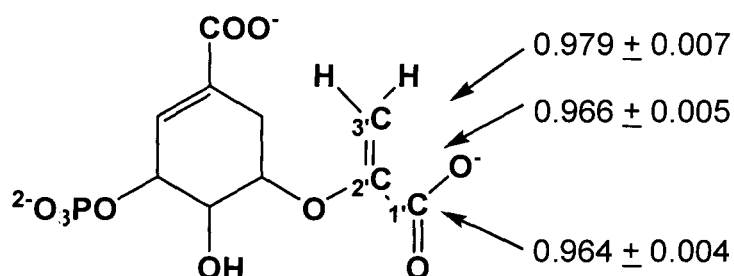


Figure 23. Summary of KIE results.

It is still possible to hypothesize as to the meaning of these results. At C1', there was a measured KIE of 0.964 ± 0.004 . There would not be any change to the bond order around this atom at the transition state, however with a positive charge at the C2' position, there could be a shortening of the bonds at the

carboxylate group, due to this ionic attraction. C3' also gave an inverse KIE of 0.979 ± 0.007 . It is going from an sp^2 to sp^3 hybridization state, and this inverse KIE would suggest that C3' has a full covalent bond formed with the proton at the TS.

The interpretation at C2' is more difficult to explain. One would expect that if a cation-like intermediate was formed, or if the reaction followed a concerted mechanism, there would be a normal isotope effect at this position. Under both these conditions, there would be a decrease in the bond order at C2', and there would be significant amounts of reaction coordinate motion as the nucleophile approached. It is therefore difficult to rationalize an inverse isotope effect if we assume that we are looking at the protonation step.

The ^2H incorporation experiment in the acid-catalyzed reaction was not done, and therefore it is not yet known whether protonation is the first irreversible step in the acid-catalyzed reaction. These KIEs therefore most likely reflect a different step later in the reaction mechanism. The step reflected by this KIE would have to be after a full bond had formed at the C2' position. This would make sense as it would reflect a step where there was more constrain around the atom, and very little reaction coordinate contribution. The step that fits these criteria would be the intramolecular proton transfer, prior to leaving group departure (Figure 24).

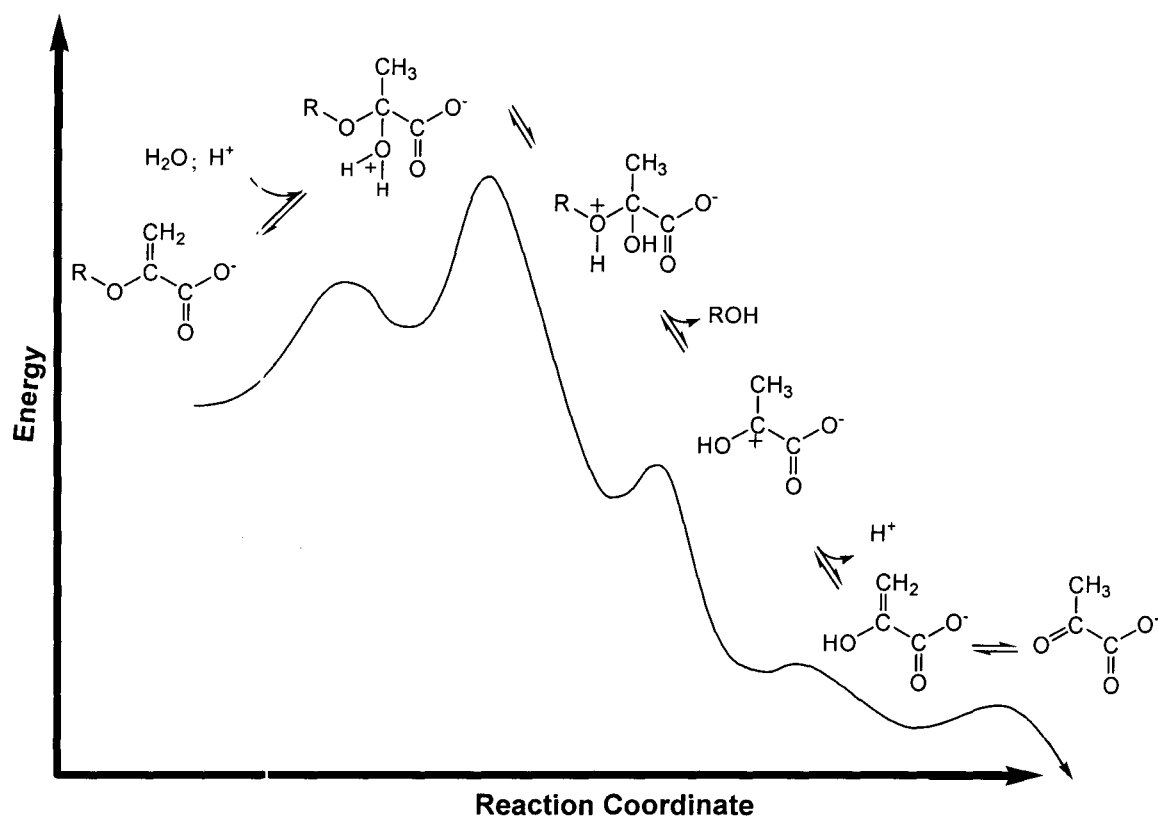


Figure 24. Reaction coordinate of Acid-catalyzed EPSP hydrolysis.

The first irreversible step of this reaction is most likely the intramolecular proton transfer, prior to leaving group departure.

Considering these initial interpretations, it is not possible to hypothesize if this reaction is following a concerted mechanism, or a stepwise mechanism. With the inverse KIE at C3', the TS is most likely fully protonated. However, since C2' is also an inverse KIE, this would suggest that at the TS, the H_2O nucleophile has already attacked the substrate. There is most likely some positively charged character at C2' which is leading to the shortening of the C-O bonds at C1', resulting in an inverse KIE at this position. It is most likely that this method is looking at a different step of the acid-catalyzed reaction compared to the AroA-catalyzed reaction. By completing the measurement of $3'\text{-}^2\text{H}$, $1'\text{-}^{18}\text{O}$ and

the bridging ^{18}O KIEs, it will be possible to complete the interpretation of these results.

These KIEs have been measured on the acid-catalyzed reaction. It will be interesting to next measure the KIEs on the AroA-catalyzed reaction. The acid-catalyzed measurements are important because they put the AroA-catalyzed results in context. The important result is how the KIEs on the AroA-catalyzed reaction differ from those of the acid-catalyzed reaction. This will precisely define the TS stabilized by the enzyme, and provide information about how to better design inhibitors for AroA.

Conclusions and Future Work

From the results obtained in the EPSP ketal study, as well as the acid-catalyzed EPSP hydrolysis study, we have provided strong support for *enolpyruvyl* activation in the AroA mechanism, leading to the formation of a cationic intermediate in the enzyme active site. This is a mechanistically relevant conclusion, as it requires > 15 kcal/mol of energy to form this cationic intermediate. If the enzyme is assisting with the stabilization of this intermediate, then it is exerting a significant amount of catalytic power to do so. If some of this binding energy could be captured in an inhibitor, this could be a good starting point for inhibitor design.

A method has been developed to measure KIEs on the acid- and enzyme-catalyzed EPSP hydrolysis reaction. KIEs on the three carbon positions of the acid-catalyzed reaction have been measured in triplicate, with good reproducibility, using liquid scintillation counting. Upon initial analysis, the vibrational environment at these three positions in the acid catalyzed reaction is becoming more constrained at the transition state, which would suggest a concerted mechanism. It will be important to compare these results to the results for the AroA-catalyzed reaction, to determine the differences in these two mechanisms.

Future work will be needed to finish the acid-catalyzed KIE measurements, then on the AroA-catalyzed reaction in the presence of SP, PGM and G6PDH.

Once these measurements are obtained, it will be possible to do a full TS analysis and understand exactly what AroA is doing to lower the activation energy of this reaction. This will provide necessary information to design an inhibitor which is a TS mimic. This could lead to the development of new drugs to treat diseases such as tuberculosis.

References

1. Robertson, J. G. (2005) Mechanistic Basis of Enzyme-Targeted Drugs, *Biochemistry* 44, 5561-5571.
2. Farmer, P. E. (2000) The consumption of the poor. Tuberculosis in the late Twentieth Century, *Ethnography* 1, 183-216.
3. Bentley, R. (1990) The Shikimate Pathway - A Metabolic Tree with Many Branches, *Crit. Rev. Biochem. Mol. Biol.* 25, 307-367.
4. Herrmann, K. M. (1995) The Shikimate Pathway as an Entry to Aromatic Secondary Metabolism, *Plant Physiol* 107, 7-12.
5. Roberts, F., Roberts, C. W., Johnson, J. J., Kyle, D. E., Krell, T., Coggins, J. R., Coombs, G. H., Milhous, W. K., Tzipori, S., Ferguson, D. J. P., Chakrabarti, D., and McLeod, R. (1998) Evidence for the Shikimate Pathway in Apicomplexan Parasites, *Nature* 393, 801-805.
6. Parish, T., and Stoker, N. G. (2002) The common aromatic amino acid biosynthesis pathway is essential in *Mycobacterium tuberculosis*, *Microbiology* 148, 3069-3077.
7. Anderson, K. S., and Johnson, K. A. (1990) Kinetic and Structural Analysis of Enzyme Intermediates: Lessons from EPSP Synthase, *Chem. Rev.* 90, 1131-1149.
8. Stallings, W. C., Abdel-Meguid, S. S., Lim, L. W., Shieh, H.-S., Dayringer, H. E., Leimgruber, R., A, Anderson, K. S., Sikorski, J. A., Padgett, S. R., and Kishore, G. M. (1991) Structure and topological symmetry of the glyphosate target 5-*enol*-pyruvylshikimate-3-phosphate synthase: A distinctive protein fold, *Proc. Natl. Acad. Sci. U S A.* 88, 5046-5050.
9. Schonbrunn, E., Eschenburg, S., Shuttleworth, W. A., Schloss, J. V., Amrhein, N., Evans, J. N. S., and Kabsch, W. (2001) Interaction of the herbicide glyphosate with its target enzyme 5-*enol*pyruvylshikimate 3-phosphate synthase in atomic detail, *Proc. Natl. Acad. Sci. U S A.* 98, 1376-1380.
10. Priestman, M. A., Healy, M. L., Becker, A., Alberg, D. G., Bartlett, P. A., Lushington, G. H., and Schonbrunn, E. (2005) Interaction of Phosphonate Analogues of the Tetrahedral Reaction Intermediate with 5-*Enol*pyruvylshikimate-3-phosphate Synthase in Atomic Detail, *Biochemistry* 44, 3241-3248.

11. Park, H., Hilsenbeck, J. L., Kim, H. J., Evans, J. N. S., and Kang, C. (2004) Structural studies of *Streptococcus pneumoniae* EPSP synthase in unliganded state, tetrahedral intermediate-bound state and S3P-GLP-bound state, *Mol. Microbiol.* **51**, 963-971.
12. Gruys, K. J., Walker, M. C., and Sikorski, J. A. (1992) Substrate Synergism and the Steady-State Kinetic Reaction Mechanism for EPSP Synthase from *Escherichia coli*, *Biochemistry* **31**, 5534-5544.
13. Gruys, K. J., Marzabadi, M. R., Pansegrau, P. D., and Sikorski, J. A. (1993) Steady-State Kinetic Evaluation of the Reverse Reaction for *Escherichia coli* 5-*enol*pyruvoylshikimate-3-phosphate Synthase, *Arch. Biochem. Biophys.* **304**, 345-351.
14. Asano, Y., Lee, J. J., Shieh, T. L., Spreafico, F., Kowal, C., and Floss, H. G. (1985) Steric course of the reactions catalyzed by 5-*enol*pyruvyshikimate-3-phosphate synthase, chorismate mutase, and anthranilate synthase, *J. Am. Chem. Soc.* **107**, 4314-4320.
15. Kim, D. H., Tucker-Kellogg, G. W., Lees, W. J., and Walsh, C. T. (1996) Analysis of Fluoromethyl Group Chirality Establishes a Common Stereochemical Course for the *Enol*pyruvyl Transfers Catalyzed by EPSP Synthase and UDP-GlcNAc *Enol*pyruvyl Transferase, *Biochemistry* **35**, 5435-5440.
16. Kim, D. H., Lees, W. J., and Walsh, C. T. (1995) Stereochemical Analysis of the Tetrahedral Adduct Formed at the Active Site of UDP-GlcNAc *Enol*pyruvyl Transferase from the Pseudosubstrates, (E)- and (Z)-3-Fluorophospho*enol*pyruvate, in D₂O, *J. Am. Chem. Soc.* **117**, 6380-6381.
17. Skarzynski, T., Kim, D. H., Lees, W. J., Walsh, C. T., and Duncan, K. (1998) Stereochemical Course of Enzymatic *Enol*pyruvyl Transfer and Catalytic Conformation of the Active Site Revealed by the Crystal Structure of the Fluorinated Analogue of the Reaction Tetrahedral Intermediate Bound to the Active Site of the C115 Mutant of MurA, *Biochemistry* **37**, 2572-2577.
18. Zemell, R. I., and Anwar, R. A. (1975) Mechanism of Pyruvate-Uridine Diphospho-V-acetylglucosamine Transferase Evidence for an Enzyme *Enol*pyruvate Intermediate, *J. Biol. Chem.* **250**, 4959-4964.
19. Brown, E. D., Marquardt, J. L., Lee, J. P., Walsh, C. T., and Anderson, K. S. (1994) Detection and Characterization of a Phospholactoyl-Enzyme Adduct in the Reaction Catalyzed by UDP-N-Acetylglucosamine *Enol*pyruvyl Transferase, MurZ, *Biochemistry* **33**, 10638-10645.

20. Anton, D. L., Hedstrom, L., Fish, S. M., and Abeles, R. H. (1983) Mechanism of Enolpyruvyl Shikimate-3-phosphate Synthase Exchange of Phosphoenolpyruvate with Solvent Protons, *Biochemistry* 22, 5903-5908.
21. Barlow, P. N., Appleyard, R. J., Wilson, B. J. O., and Evans, J. N. S. (1989) Direct observation of the enzyme-intermediate complex of 5-enolpyruvylshikimate-3-phosphate synthase by ^{13}C NMR spectroscopy, *Biochemistry* 28, 7985-7991.
22. Bondinell, W. E., Vnek, J., Knowles, P. F., Sprecher, M., and Sprinson, D. B. (1971) On the Mechanism of 5-Enolpyruvylshikimate 3-Phosphate Synthetase, *J. Biol. Chem.* 246, 6191-6196.
23. Grimshaw, C. E., Sogo, S. G., and Knowles, J. R. (1982) The Fate of the Hydrogens of Phosphoenolpyruvate in the Reaction Catalyzed by 5-Enolpyruvylshikimate-3-phosphate Synthase, *J. Biol. Chem.* 257, 596-598.
24. Anderson, K. S., Sikorski, J. A., and Johnson, K. A. (1988) A Tetrahedral Intermediate in the EPSP Synthase Reaction Observed by Rapid Quench Kinetics, *Biochemistry* 27, 7395-7406.
25. Anderson, K. S., Sikorski, J. A., Benesi, A. J., and Johnson, K. A. (1988) Isolation and Structural Elucidation of the Tetrahedral Intermediate in the EPSP Synthase Enzymatic Pathway, *J. Am. Chem. Soc.* 110, 6577-6579.
26. Anderson, K. S., and Johnson, K. A. (1990) "Kinetic competence" of the 5-enolpyruvylshikimate-3-phosphate synthase tetrahedral intermediate, *J. Biol. Chem.* 265, 5567-5572.
27. Byczynski, B., Mizyed, S., and Berti, P. J. (2003) Nonenzymatic Breakdown of the Tetrahedral (α -Carboxyketol Phosphate) Intermediates of MurA and AroA, Two Carboxyvinyl Transferases. Protonation of Different Functional Groups Controls the Rate and Fate of Breakdown, *J. Am. Chem. Soc.* 125, 12541-12550.
28. Anderson, K. S., Sammons, R. D., Leo, G. C., and Sikorski, J. A. (1990) Observation by ^{13}C NMR of the EPSP synthase tetrahedral intermediate bound to the enzyme active site, *Biochemistry* 29, 1460-1465.
29. Marquardt, J. L., Brown, E. D., Walsh, C. T., and Anderson, K. S. (1993) Isolation and Structural Elucidation of a Tetrahedral Intermediate in the UDP-N-acetylglucosamine Enolpyruvyl Transferase Enzymatic Pathway, *J. Am. Chem. Soc.* 115, 10398-10399.

30. Kim, D. H., Lees, W. J., and Walsh, C. T. (1994) Formation of Two Enzyme-bound Reaction Intermediate Analogs during Inactivation of UDP-GlcNAc Enolpyruvyl Transferase by (E)- or (Z)-3-Fluorophosphoenolpyruvate, *J. Am. Chem. Soc.* **116**, 6478.
31. Kim, D. H., Lees, W. J., Kempell, K. E., Lane, W. S., Duncan, K., and Walsh, C. T. (1996) Characterization of a Cys115 to Asp Substitution in the Escherichia coli Cell Wall Biosynthetic Enzyme UDP-GlcNAc Enolpyruvyl Transferase (MurA) That Confers Resistance to Inactivation by the Antibiotic Fosfomycin, *Biochemistry* **35**, 4923-4928.
32. Leo, G. C., Sikorski, J. A., and Sammons, R. D. (1990) Novel Product from EPSP Synthase at Equilibrium, *J. Am. Chem. Soc.* **112**, 1653-1654.
33. Schonbrunn, E., Sack, S., Eschenburg, S., Perrakis, A., Krekel, F., Amrhein, N., and Mandelkow, E. (1996) Crystal structure of UDP-N-acetylglucosamine enolpyruvyltransferase, the target of the antibiotic fosfomycin, *Structure* **4**, 1065.
34. Skarzynski, T., Mistry, A., Wonacott, A., Hutchinson, S. E., Kelly, V. A., and Duncan, K. (1996) Structure of UDP-N-acetylglucosamine enolpyruvyl transferase, an enzyme essential for the synthesis of bacterial peptidoglycan, complexed with substrate UDP-Nacetylglucosamine and the drug fosfomycin, *Structure* **4**, 1465-1474.
35. Zhang, F., and Berti, P. J. (2006) Phosphate Analogues as Probes of the Catalytic Mechanisms of MurA and AroA, Two Carboxyvinyl Transferases, *Biochemistry* **45**, 6027-6037.
36. Mized, S., Wright, J. E. I., Bczynski, B., and Berti, P. J. (2003) Identification of the Catalytic Residues of AroA (Enolpyruvylshikimate 3-Phosphate Synthase) Using Partitioning Analysis, *Biochemistry* **42**, 6986-6995.
37. Eschenburg, S., Kabsch, W., Healy, M. L., and Schonbrunn, E. (2003) A New View of the Mechanisms of UDP-N-Acetylglucosamine Enolpyruvyl Transferase (MurA) and 5-Enolpyruvylshikimate-3-phosphate Synthase (AroA) Derived from X-ray Structures of Their Tetrahedral Reaction Intermediate States, *J. Biol. Chem.* **278**, 49215-49222.
38. An, M., Maitra, U., Neidlein, U., and Bartlett, P. A. (2003) 5-Enolpyruvylshikimate 3-Phosphate Synthase: Chemical Synthesis of the Tetrahedral Intermediate and the Assignment of the Stereochemical Course of the Enzyme Reaction, *J. Am. Chem. Soc.* **125**, 12759-12767.

39. Priestman, M. A., Healy, M. L., Funke, T., Becker, A., and Schonbrunn, E. (2005) Molecular basis for the glyphosate-insensitivity of the reaction of 5-enolpyruvylshikimate 3-phosphate synthase with shikimate, *FEBS Lett.* **579**, 5773-5780.
40. Steinrucken, H. C., and Amrhein, N. (1980) The Herbicide Glyphosate is a Potent Inhibitor of 5-Enolpyruvyl-Shikimic Acid-3-Phosphate Synthase, *Biochem. Biophys. Res. Commun.* **94**, 1207-1212.
41. Boocock, M. R., and Coggins, J. R. (1983) Kinetics of 5-enolpyruvylshikimate-3-phosphate synthase inhibition by glyphosate, *FEBS Lett.* **154**, 127- 133.
42. Steinrucken, H. C., and Amrhein, N. (1984) 5-Enolpyruvylshikimate-3-phosphate synthase of *Klebsiella pneumoniae* 2. Inhibition by glyphosate [N-(phosphonomethyl)glycine], *Eur. J. Biochem* **143**, 351-357.
43. Sammons, R. D., Gruys, K. J., Anderson, K. S., Johnson, K. A., and Sikorski, J. A. (1995) Reevaluating Glyphosate as a Transition-State Inhibitor of EPSP Synthase: Identification of an EPSP Synthase:EPSP.Glyphosate Ternary Complex, *Biochemistry* **34**, 6433-6440.
44. Garcia-Alles, L. F., and Erni, B. (2002) Synthesis of phosphoenol pyruvate (PEP) analogues and evaluation as inhibitors of PEP-utilizing enzymes, *Eur. J. Biochem* **269**, 3226-3236.
45. Alberg, D. G., Lauhon, C. T., Nyfeler, R., Fassler, A., and Bartlett, P. A. (1992) Inhibitor of EPSP Synthase by Analogues of the Tetrahedral intermediate and of EPSP, *J. Am. Chem. Soc.* **114**, 3535-3546.
46. Alberg, D. G., and Bartlett, P. A. (1989) Potent Inhibition of 5-Enolpyruvylshikimate-3-phosphate Synthase by a Reaction Intermediate Analogue, *J. Am. Chem. Soc.* **111**, 2337-2338.
47. Tinoco Jr, I., Sauer, K., and Wang, J. C. (1995) in *Physical Chemistry: Principles and Application in Biological Sciences* (Tinoco Jr, I., Sauer, K., and Wang, J. C., Eds.) pp 369-371, Prentice Hall, New Jersey.
48. Roberts, R. B., Cowie, D. B., Abelson, P. H., Bolton, E. T., and Britten, R. J. (1963) *Studies of biosynthesis in Escherichia coli*, Vol. Publication 607, Carnegie Institute of Washington, Washington, DC.
49. Guthrie, R. D., and Jencks, W. P. (1989) IUPAC Recommendations for the Representation of Reaction Mechanisms, *Acc. Chem. Res.* **22**, 343-349.

50. Berti, P. J. (1999) Determining Transition States from Kinetic Isotope Effects, *Methods Enzymol* 308, 355-397.
51. Berti, P. J., and McCann, J. A. B. (2006) Toward a Detailed Understanding of Base Excision Repair Enzymes: Transition State and Mechanistic Analyses of N-Glycoside Hydrolysis and N-Glycoside Transfer, *Chem. Rev.* 106, 506-555.
52. Parkin, D. W. (1991) in *Enzyme Mechanism from Isotope Effects* (Cook, P. F., Ed.) pp 269-290, CRC Press Inc., Boca Raton, Florida.
53. Unrau, P. J., and Bartel, D. P. (2003) An oxocarbenium-ion intermediate of a ribozyme reaction indicated by kinetic isotope effects, *Proc. Natl. Acad. Sci. U S A.* 100, 15393-15397.
54. Weiss, P. M. (1991) in *Enzyme Mechanism from Isotope Effects* (Cook, P. F., Ed.) pp 291-311, CRC Press Inc, Boca Raton, Florida.
55. Lee, J. K., Bain, A. D., and Berti, P. J. (2004) Probing the Transition States of Four Glucoside Hydrolyses with ¹³C Kinetic Isotope Effects Measured at Natural Abundance by NMR Spectroscopy, *J. Am. Chem. Soc.* 126, 3769-3776.
56. Pace, C. N., Vajdos, F., Fee, L., Grimsley, G., and Gray, T. (1995) How to measure and predict the molar absorption coefficient of a protein, *Protein Science* 4, 2411-2423.
57. Anderson, K. S., Sikorski, J. A., and Johnson, K. A. (1988) Evaluation of 5-Enolpyruvylshikimate-3-phosphate Synthase Substrate and Inhibitor Binding by Stopped-Flow and Equilibrium Fluorescence Measurements, *Biochemistry* 27, 1604-1610.
58. Anderson, K. S., Sikorski, J. A., and Johnson, K. A. (1988) A tetrahedral intermediate in the EPSP synthase reaction observed by rapid quench kinetics, *Biochemistry* 27, 7395-7406.
59. Barshop, B. A., Wrenn, R. F., and Frieden, C. (1983) Analysis of numerical methods for computer simulation of kinetic processes: development of KINSIM - a flexible, portable system, *Anal. Biochem.* 130, 134-145.
60. Zimmerle, C. T., and Frieden, C. (1989) Analysis of progress curves by simulations generated by numerical integration, *Biochem J* 258, 381-387.

61. Berti, P. J., Blanke, S. R., and Schramm, V. L. (1997) Transition State Structure for the Hydrolysis of NAD⁺ Catalyzed by Diphtheria Toxin, *J. Am. Chem. Soc.* *119*, 12079-12088.
62. Barshop, B. A., Wrenn, R. F., and Frieden, C. (1983) Analysis of numerical methods for computer simulation of kinetic processes: Development of KINSIM--A flexible, portable system, *Anal. Biochem.* *130*, 134-145.
63. Zimmerle, C. T., and Frieden, C. (1989) Analysis of progress curves by simulations generated by numerical integration, *Biochem. J.* *258*, 381-387.
64. Kresge, A. J., Leibovitch, M., and Sikorski, J. A. (1992) Acid- Catalyzed Hydrolysis of 5 - Enolpyruvylshikimate 3-Phosphate (EPSP) and Some Simple Models of Its Vinyl Ether Functional Group, *J. Am. Chem. Soc.* *114*, 2618-2622.